

# **Doctoral Thesis**

## **A Study on Long-Lifetime Excited 3d electron States of Zinc Atoms Generated by Surface Ion-recombination Processes**

**Li CHEN**

**Kagoshima University  
March 2015**

# Contents

|                  |   |           |
|------------------|---|-----------|
| <b>Chapter 1</b> | <b>Introduction.....</b>  | <b>4</b>  |
| 1.1              | Background of our research.....   | 4         |
| 1.2              | The researching object.....   | 7         |
| 1.2.1            | The periodic table.....   | 7         |
| 1.2.2            | The excited state of Zn <sub>2</sub> with long lifetime.....  | 9         |
| 1.3              | Significance and purpose of the research.....   | 10        |
| <b>Chapter 2</b> | <b>Generated Process and Experiment.....</b>  | <b>11</b> |
| 2.1              | The deposition system apparatus.....  | 11        |
| 2.2              | The ion-recombination process field.....  | 13        |
| 2.2.1            | The reaction field.....   | 13        |
| 2.2.2            | Ion-recombination process.....  | 14        |
| 2.3              | Surface electron distribution.....  | 15        |
| <b>Chapter 3</b> | <b>Excited State Depend on Energy.....</b>  | <b>17</b> |
| 3.1              | The selection rule.....   | 17        |
| 3.2              | The Results of XRD.....   | 18        |
| 3.3              | Intensity of diffuse scattering and Bragg diffraction depend on<br>irradiation electron energy..... | 19        |
| 3.4              | Energy dependence and excited type of zinc.....   | 22        |
| 3.5              | The properties of excited zinc films.....   | 23        |
| <b>Chapter 4</b> | <b>The Theories.....</b>  | <b>24</b> |
| 4.1              | The excited state.....  | 24        |
| 4.2              | Interaction of polarization coordination.....   | 26        |
| 4.3              | X-ray photoelectron spectroscopy (XPS).....   | 28        |
| 4.3.1            | What is x-ray photoelectron spectroscopy? .....   | 28        |
| 4.3.2            | Charge transfer (CT) in Transition Metal (TM).....  | 30        |
| 4.3.3            | Hund's rules and final state effects of atomic multiplets.....                                      | 33        |
| 4.3.4            | Initial state and final state of TM.....  | 34        |
| 4.4              | The 2p XPS of TM.....   | 37        |

|  |           |
|--|-----------|
| 4.5 Charge transfer in TM (CuO and Cu).....                            | 39        |
| 4.6 Theoretical calculations of the charge transfer parameters.....    | 42        |
| <b>Chapter 5 The Proof of excited Zinc by XPS.....</b>                 | <b>46</b> |
| 5.1 XPS result of 9 vertical points at the center of “Sample 100”..... | 47        |
| 5.2 Analysis of XPS spectra.....                                       | 49        |
| 5.3 Discussion .....   | 52        |
| 5.3.1 The states of zinc.....  | 52        |
| 5.3.2 Theoretical Calculation of CT.....                               | 54        |
| 5.3.3 The spatial symmetry of excited zinc film.....                   | 55        |
| 5.3.4. The Structural instability of Excited Zn Film.....              | 56        |
| <b>Chapter 6 The Correlation Between Elements.....</b>                 | <b>57</b> |
| 6.1 The results of 192 points by XPS.....                              | 57        |
| 6.2 The correlation between constituent elements.....                  | 59        |
| 6.3 The time and spatial distribution of films.....                    | 61        |
| <b>Chapter 7 Conclusions.....</b>                                      | <b>63</b> |
| <b>Reference.....</b>  | <b>64</b> |
| <b>Main Thesis.....</b>  | <b>67</b> |
| <b>Acknowledgements.....</b>   | <b>69</b> |

# *Chapter 1 INTRODUCTION*

## *1.1 Background of Our Research*

### *Society request:*

Throughout the history of human society, there were three times large change in the society. Firstly, agricultural society that was able to tool of constant quality from hunting society using natural. Secondly, it is an industrial society in which, the industrial revolution was happened. In a nutshell, from the society, which is based agriculture (traditional agriculture), transition to a society which is based Industries (modern industry). Thirdly, the information society right now, caused by mass production, under the influence of the large amount of consumption of industrial society, the problem of global warming, and energy depletion is significantly, limits to growth has been seen. To exceed this limit, we have pursued to a friendly to environment new concept technologies to be introduce. [1]

### *The limit of materials science:*

The characteristic of materials caused to the outer shell electrons. Inner shell electrons localized at atom, therefore, the characteristic of materials independent on the inner shell electrons. There are various materials, and there are various functions in materials. Conductor material, semiconductor material, such as solid electrolyte conductor material is focused on (moving of electron, hole and ion) electrical conductivity; Magnet and hard disk is to focus on (an array of magnetic moment) of magnetic material; Catalyst, and photo-catalyst is focus on optical properties and the nature of the material surface. The properties of material are determined by the spacing between the atoms and the arrangement of atoms and so on, what determined in the element types, creation schemes, condition of secondary processing and so on. Physical properties of the material had been determined by the operation (the valence band, conduction band) of the outer shell electronic. The functionality of the chemical industry in the 20 century, it revolves around the electronic materials, including semiconductor, member market has been expanding due

to the growing market of the product. In order to improve the physical properties of the material, it was realized by controlling the state of the electrons in the low binding energy level of the valence band and the conduction band. In other words, materials research up to now was the operation of the outer shell electrons. [2]

### ***The limit of material technology:***

As referred to "miniaturization of semiconductor products", there is a limit in the sense of semiconductor technology. However, because I think that there is no limit of the "general semiconductor technology" in "academic". With respect to the former, I will describe with respect to the limit in some perspective. [3] [4]

In order to make a semiconductor, it is required technique to make exactly a fine pattern. However, gate size of the current state-of-the-art is off to a  $0.1\mu\text{m}$ , 65nm and 90nm. However lights for machining, and this utilizes a wavelength greater than the process size KrF (248nm), ArF (193nm), and F2 (157nm), in an excimer laser and 365nm in i-line. Therefore, we design that takes into account the interference of light now. Without (the wavelength is also is the X-ray region) only make use of a large-scale X-ray exposure when it comes to the size reduction of more, it is no longer afford to not say easily manufactured.

The transistor of minimum size of the current is sized to control the flow of electrons of several tens to several hundred electrons. When it comes to less than this, it is no longer at the level considered "current", and it becomes to deal with the wave function "electronic" level. Of course, this area something like SET (Single Electron Transistor) also has been studied. Although it is possible reduction of this size or less, because it will be different with the concept of the transistor so far, so circuit design is no longer simple. Furthermore, considering the malfunction by temperature, in theory, it is possible to drop the control voltage to 0.2V (potential higher than  $kT$ ) , but consider the change in the control voltage due to the reduced size of the processing, the limit may be close.

When you look back on the history of semiconductor products on the transistor using Si material, in particular, there is no doubt that "miniaturization" is an important keyword. With the miniaturization, processing performance of the transistor increases dramatically to between 50

years, the size was smaller and smaller. The miniaturization of semiconductor has been underpinned the development of electronics. However, in the 21 century, the situation has changed. The results of continued miniaturization is that, problems due to the physical properties of the transistor is evident, the extension of the previous techniques, it is possible to promote miniaturization is upon getting harder. New study was introduced into the logic circuit, what has not been used in the world of logic circuit so far to resolve for this problem, the ferroelectric material and a magnetic material, rather than aim for miniaturization, and add a new value in the new material like the spintronic insulator and topological insulator.

### ***Development of innovative material:***

According to an article in Nature Nanotechnology "Traditional (electronic) materials reached the limit, and it will be replaced by a completely new material, and new device structure has come to be required. The structure and new materials of these, MOS device less future would keep the market of 10 years, but the performance improvements in later, a whole new computing paradigm device structures and nanowires, and molecular devices must almost certainly will become more ". Although there are many studies on excited state excited inner-shell electrons, but it is the study of quantum mechanical theory almost, not a study suited to take advantage of the physical chemistry traditional. Our group aims to control the inner shell electrons' new materials development innovative technology. Because it exceeds the limit of physical laws and limitations of the manufacturing technology, new research subjects spintronics, such as topology insulator has produced, but stand in that it aims at different research and application of the outer electrons of up to now, this study group the inner shell electron the standpoint of the application of chemical, I conducted a study of zinc thin film excited inner-shell electron of long life for the (Zn excimer). It is expected that this study will provide significant contribution to the basic technology of new materials creation.

## 1.2 The Researching Object

About why we select zinc to be our researching object element, there are two most important reasons. Firstly, the special position of Zn in periodic table. Zinc is a 3d full filled transition metal. Secondly, spontaneous lifetime of molecular  $Zn_2$  to  $2Zn$  atoms is very long. Also, from bound excited states of  $Zn_2$  to the ground state could be longer than other elements.

### 1.2.1 The periodic table

Table 1.1 The outer shell electron configuration of transition metals [5]

| The Periodic Table                   |                  |                  |                   |                   |                   | B               | C               |
|--------------------------------------|------------------|------------------|-------------------|-------------------|-------------------|-----------------|-----------------|
| Electron configuration (outer shell) |                  |                  |                   |                   |                   | 2p <sup>1</sup> | 2p <sup>2</sup> |
|                                      |                  |                  |                   |                   |                   | Al              | Si              |
| Mn                                   | Fe               | Co               | Ni                | Cu                | Zn                | Ga              | Ge              |
| d5s <sup>2</sup>                     | d6s <sup>2</sup> | d7s <sup>2</sup> | d8s <sup>2</sup>  | d10s <sup>1</sup> | d10s <sup>2</sup> | 4p <sup>1</sup> | 4p <sup>2</sup> |
| Tc                                   | Ru               | Rh               | Pd                | Ag                | Cd                | In              | Sn              |
| d5s <sup>2</sup>                     | d7s <sup>1</sup> | d8s <sup>1</sup> | d10s <sup>0</sup> | d10s <sup>1</sup> | d10s <sup>2</sup> | 5p <sup>1</sup> | 5p <sup>2</sup> |
| Re                                   | Os               | Ir               | Pt                | Au                | Hg                | Tl              | Pb              |
| d5s <sup>2</sup>                     | d6s <sup>2</sup> | d7s <sup>2</sup> | d9s <sup>1</sup>  | d10s <sup>1</sup> | d10s <sup>2</sup> | 6p <sup>1</sup> | 6p <sup>2</sup> |

Cu: 3d<sup>10</sup>4s<sup>1</sup>

Zn: 3d<sup>10</sup>4s<sup>2</sup>

Cu<sub>2</sub>O: 3d<sup>10</sup>4s<sup>0</sup>

ZnO: 3d<sup>10</sup>4s<sup>0</sup>

CuO: 3d<sup>9</sup>4s<sup>0</sup>

Zn-X: 3d<sup>9</sup>4s<sup>0</sup>

X:ligand

In periodic table was showed in fig.1.1, Zn is a typical metal nearby transition metal. Elements in the periodic table can be divided into nonmetal, semi-metal and metal, furthermore, metal includes typical metal and transition metal. The atomic position of elements in the periodic table is decided by the atom ordinal and electronic arrangement. Physical and chemical properties of the elements in the periodic table is closely related to the position of elements, in other words, the nature of elements is closely related to its atomic number and electronic arrangement. In table.1, electronic configuration of transition metals and these oxides of elements Co, Ni, Cu and typical metals and these oxides of elements Zn, Ga was showed [6][7]. The d block metal (transition metal) with  $d^n(n=1\sim 9)$  like Co, Ni; The f block metal (transition metal) with  $f^n(n=1\sim 13)$  like Rh, Pd; The p block metal (typical metal) with  $d^n(n=0$  or  $n=10)$  like ZnO, Ga<sub>2</sub>O<sub>3</sub>. About strongly correlated electron system, just f and d orbital's electrons of rare earth and transition metal atoms are utilized. In strongly correlated electron system of transition metal (CoO, NiO, CuO), the d shell is unclosed and d orbital is filled

with  $n$  electrons ( $n < 10$ ). If the p block metal is excited to  $d^n (n < 10)$  from  $d^n (n = 10)$  (inner hole excitation or 3d electron excitation), coulomb interactions could be increased. That means typical metal could show strongly correlated electron system. The essence of the nanotechnology, researching and development of composite materials and so on are controlling the outer shell electrons. Our opinion of controlling the inner shell electrons (in this paper is 3d electrons of zinc) of material modification technique has very important significance.

**Table 1.2 Electron configurations of transition metal and metal oxide.**

| Element   | Metal   | Metal Oxide  |
|-----------|---|--|
| $^{27}Co$ | $Co: [Ar]3d^7 4s^2$   | $CoO: [Ar]3d^7 4s^0$   |
| $^{28}Ni$ | $Ni: [Ar]3d^8 4s^2$   | $NiO: [Ar]3d^8 4s^0$   |
| $^{29}Cu$ | $Cu: [Ar]3d^{10} 4s^1$  | $CuO: [Ar]3d^9 4s^0$<br>$Cu_2O: [Ar]3d^{10} 4s^0$                  |
| $^{30}Zn$ | $Zn: [Ar]3d^{10} 4s^2$<br>$Zn^*: [Ar]3d^9 4s^2 4p^1$<br>$Zn^{*2}: [Ar]3d^8 4s^2 4p^2$ | $ZnO: [Ar]3d^{10} 4s^0$  |
| $^{31}Ga$ | $Ga: [Ar]3d^{10} 4s^2 4p^1$   | $Ga_2O: [Ar]3d^{10} 4s^2 4p^0$<br>$Ga_2O_3: [Ar]3d^{10} 4s^0 4p^0$ |

### 1.2.2 The excited state of molecular Zn<sub>2</sub> with long lifetime

Calculated and experimental spontaneous lifetimes of the Zn from molecular Zn<sub>2</sub> were 1.1ns and 1.41ns of state <sup>1</sup>P<sub>1</sub>; Lifetimes of states <sup>3</sup>P<sub>1</sub> were 6.2μs and 20.μs. To Hg <sup>1</sup>P<sub>1</sub>, calculated and experimental spontaneous lifetimes of Hg from molecular Hg<sub>2</sub> were 0.67ns and 1.31ns; Lifetimes of states Hg<sub>2</sub> <sup>3</sup>P<sub>1</sub> were 68.ns and 114.ns. Spontaneous lifetime of molecular Zn<sub>2</sub> at state <sup>3</sup>P<sub>1</sub> is in micro second (μs) order. Most lifetimes of inner core bound excited states of elements is ns order. The transition moments and lifetimes for the dipole allowed transitions from bound excited states of Zn<sub>2</sub> and “Hg<sub>2</sub>” to the ground state with spin-orbit coupling were shown in table.1. The transition processes  $1_u( {}^3\Sigma_u^+ ) \rightarrow 0_g^+$  of Zn<sub>2</sub> have the longest lifetime 16μs. The excitation state  $1_u( {}^3\Sigma_u^+ )$  of Zn<sub>2</sub> showed quasi-stable.

**Table 1.3 Transition moments and lifetimes for the dipole allowed transitions from bound excited states of Zn<sub>2</sub> and Hg<sub>2</sub> to the ground state. [8]**

| State                                       | Zn <sub>2</sub> | Hg <sub>2</sub> |
|---|-----------------|-----------------|
| $1_u( {}^3\Sigma_u^+ ) \rightarrow 0_g^+$   | 16. μs          | 35. ns          |
| $1_u( {}^1\Pi_u ) \rightarrow 0_g^+$        | 0.52 ns         | 0.34 ns         |
| $0_u^+( {}^1\Sigma_u^+ ) \rightarrow 0_g^+$ | 0.52 ns         | 0.34 ns         |

### ***1.3 Significance and Purpose of the Research***

In the vapor deposition process, having a surface ion recombination, the present study is on new generated of zinc excited. First, it was demonstrated that the elucidation of data EPMA and XPS, zinc is excited performs charge transitions were multiple splitting of Zn3d8. Next, the elucidation of the data XPS, EPMA, SEM, Laser Raman and etc., shows a special behavior of the excitation of zinc, were elucidated.[9][10]

Technique in materials chemistry is due to control of the most outer shell electron, From the standpoint of materials chemistry, study of new materials creation under the control of the inner shell electron is scarcely. Control of inner-shell electron is involved in the excitation process and the relaxation process. About these processes, there are a lot of researches. The excimer in the excited state is derived from excited dimer for short. Excimer is the electron excited states atoms and molecules in combination with other atoms and molecules. The lifetime of an excimer is very short, on the order of nanoseconds. Binding of a larger number of excited atoms form Rydberg matter clusters, the lifetime of which can exceed many seconds [1]. As we all know, the transition metal group has special un-full filled 3d electronic configuration. And zinc ( $\Pi_b$ ) is the only full-filled 3d electronic configuration of transition metal elements. So, our group is focused on creating permanent lifetime zinc excimer, learning the mechanism formation processes and analysis the results phenomenon. The excitation can be exploited in modification of the surface layers, modification of the bulk in a selected way, energy transport and charge transport, energy storage and so on. The chemical reactions depend on the number of outer electrons in usually; however, if we can arrange the inner-core electron system of the atom, we can get a new periodic table, that is, new development platform.

# *Chapter 2    GENERATED PROCESS AND EXPERIMENT*

## *2.1 The Deposition System Apparatus*

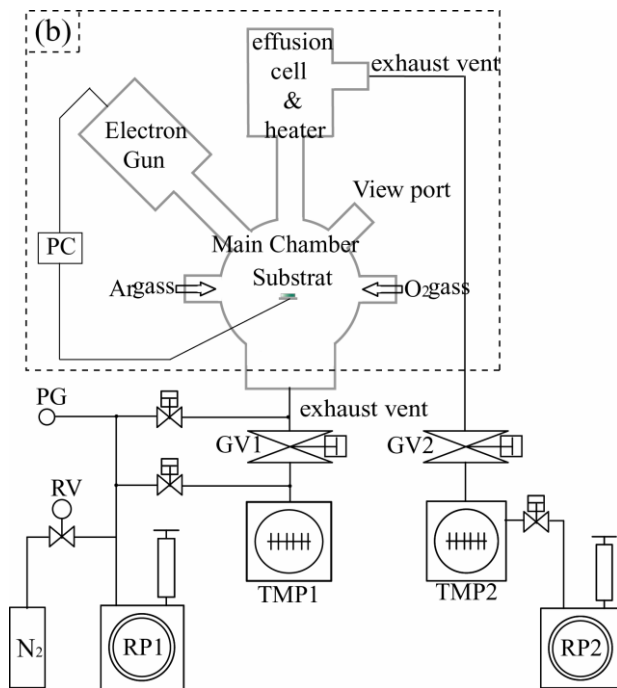


**Fig.2.1 Schematic illustration of an apparatus [19]**

The experiment apparatus which was developed just by our research group is an integral evaporation system with transmission electron spectroscopy evaluation (Electron-assisted PVD) in fig.2.1. The arrangement is arranged to input and output ports 5 to 45° intervals. They are electron gun of thermionic emission, heating cell deposition of raw materials (zinc), view port, the Ar gas by the mass flow controller and as well as O<sub>2</sub> gas input ports. Mounting the slit can be controlled motor to the input-output ports, and block the incoming gas and the incident electrons. Furthermore, in order to prevent the generation of particles by the rotation mechanism and the residual gas, and raising the degree of vacuum by differential pumping by the molecular pump.

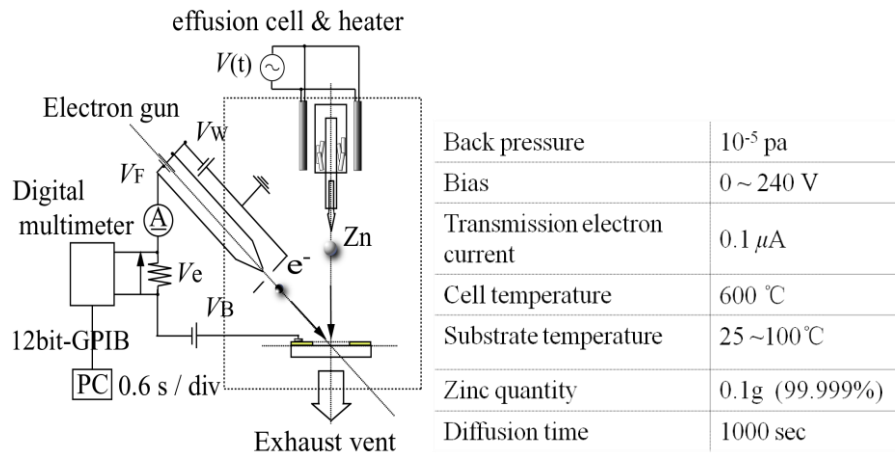


**Fig.2.2 Conceptual diagram of the transmission electron spectroscopy, evaluation integrated deposition system and the main experiments condition. [19]**

Conceptual diagram of the transmission electron spectroscopy, evaluation integrated deposition system and the main experiments condition were showed in fig.2.2. The thermal electrons, what emitted from the tungsten filament hairpin, such as SEM, was used as the incident electron source. In addition, manganese battery is used as wehnelt voltage and  $V_w=9.6\text{V}$ . Thermal electrons emitted from the electron gun be accelerated by the bias voltage ( $V_B = 0 \sim 240\text{V}$ ), what applied to the substrate electrode, and thermal electrons irradiate a wide range to the substrate surface. The incident angle of electrons was  $45^\circ$  from the substrate surface, Then the zinc atoms were deposited on the insulate area from the effusion cell at  $600^\circ\text{C}$ , and the insulate area is measured about  $R=3.5\text{mm}$  in diameter at the center of the sapphire substrate.

## 2.2 The Ion-recombination Process Field

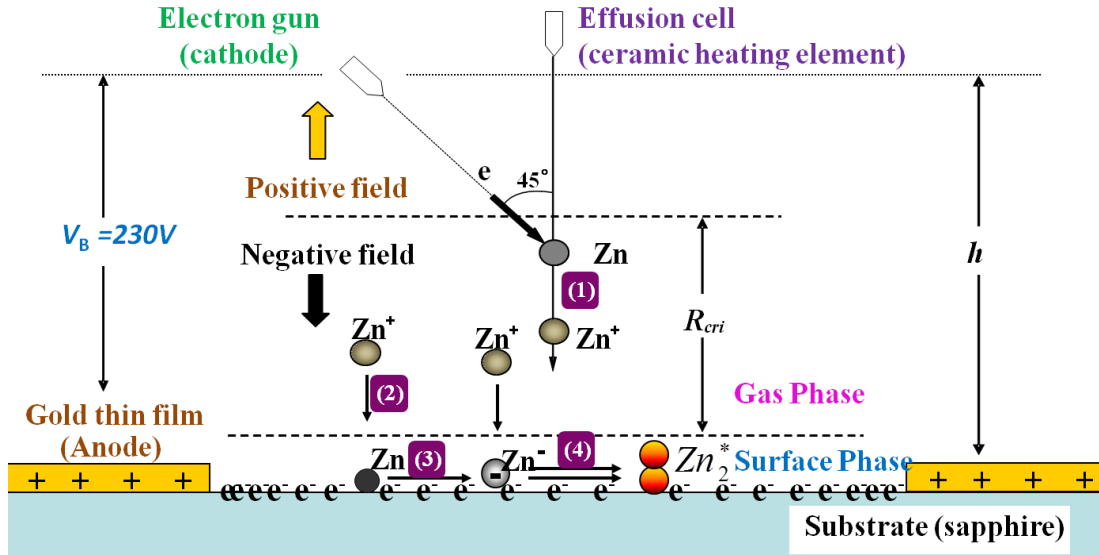


Fig.2.3 Conceptual diagram of the reaction spaces [16], [17].

### 2.2.1 The reaction field:

Fig.2.3 is a conceptual diagram of the reaction field. From figure 1 and 2: at the peripheral portion of the oxide aluminum substrate, equipped with a gold film in order to provide a bias voltage of the incident electrons. When the bias voltage added from electron gun (cathode) to gold thin film (anode), the reaction field became an electric field and vector of this electric field is from gold thin film to electron gun. Clone force  $\mathbf{F}$  acting on the point charge is write by  $\mathbf{F} = Q\mathbf{E}$ , at first, acting a clone force from electron gun toward gold thin film to the incident electron, with the sapphire substrate, the incident electron can adhere on the sapphire. Then, electrons have been accumulating on top of the substrate (Adhesion electrons create a potential/field at the substrate surface.), number of adhered electrons have been increasing until potential of the substrate surface to  $-V_B$ . Now, a stable and downward electric field has been created by adhered electrons. Initial velocity of incident zinc particles is downward. Zinc particles only have momentum in the vertical direction. The sapphire surface was electrified by incident electrons up to the same magnitude of potential as the anode bias. This growth field makes selective

growth field for Zn<sup>+</sup>.

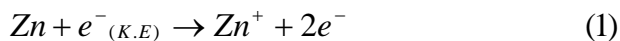
Electrons form a stable and substrate orientation electric field at the center of oxide aluminum substrate where radius R=3.5mm. Corresponds to thermal electrons emitted from the electron gun be accelerated by the bias voltage ( $V_B = 0 \sim 240V$ ), the potential of the insulating portion is negative and its absolute value is equal to the bias potential  $V_B$ . Corresponds to the bias potential, the electrons that in the reaction field have a stability energy and it equal total of potential energy and kinetic energy ( $E_e = E_p + E_k$ ). And the electrons on the substrate must have a potential energy of 0~240eV. In other words, incident electronic energy should be 0~240eV. By the quantum theory, the possible energy value of atoms is discrete. Then, when the transition to the (excited state) high energy state from low energy state, just excitation energy of discrete energy difference  $\Delta E = E_2 - E_1$  is required.

### ***2.2.2 Ion-recombination process:***

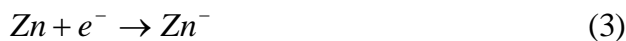
In a vapor phase growth processes, kinetic energy of incident atoms in the gas phase were dissipated at the surface phase in the condensation processes [18]. Zinc excimers were formed on sapphire substrates within diameter of 6.5mm area, where enclosed by gold electrode, which is the anode for incident electrons exciting zinc atoms. An estimate excited process of zinc thin films included 4 steps:

*Charging process :*

*Ionization :*



*Electron Attachment :*



*Ion – Re combination :*



Firstly, zinc that incidence from effusion cell is ionized by incidence electron in the negative field (1) in the gas phase, lifetime of Zn<sup>+</sup> can be extended by the electric field; Secondly, the ionized Zn<sup>+</sup> adhered to the substrate (surface of sapphire), and adhered Zn<sup>+</sup> combined with electron to Zn at substrate

surface (2); Thirdly, Zn combined with electron to Zn<sup>-</sup> at substrate (3). Lastly, Zn<sup>-</sup> what adhered at substrate combined with Zn<sup>+</sup> what come from negative field and excited state formed (4). Lifetime of negative ions is much shorter than positive ions. An electron charged up sapphire surface was used to elongate the lifetime of Zn<sup>-</sup>. Normally, lifetime of excimer is transitory, counting as ns, but excited zinc atoms are from surface phase fixed in solid phase at the first period, so that, the excited states were preserved for a long time. We daring assumed that the excited zinc was created though the special charging field due to ion-recombination processes. Electron density distribution determined the density of excited zinc.

### ***2.3 Surface Electron Distribution***

Surface electron distribution was simulated in fig.2.4 and fig.2.5. The surface electron distribution was simulated by Microsoft Visual Basic 6.0 (Attach 1). 870 electrons were evenly sprinkled on the circular plate (substrate), R=2000 in fig.2.4a. Then charge intensity is similar on the substrate in fig.2.4b. The potential distribution was simulated in fig.2.4c. Potential at center of substrate is highest, and at the edge of the substrate is lowest. In multi-electron system, electrons number n=870, the potential U at P is:

$$U = \frac{Q_1}{4\pi\epsilon_0 r_1} + \frac{Q_2}{4\pi\epsilon_0 r_2} + \dots + \frac{Q_{870}}{4\pi\epsilon_0 r_{870}} \quad (5)$$

If P with electricity Q, the electric force by the superposition of the electric field at P is:

$$F = QE = Q \frac{U}{E} = Q \left( \frac{QQ_1}{4\pi\epsilon_0 r_1^2} + \frac{QQ_2}{4\pi\epsilon_0 r_2^2} + \dots + \frac{QQ_{870}}{4\pi\epsilon_0 r_{870}^2} \right) \quad (6)$$

The electric at P shift by electric force F. At last, electric force F=QE=0 and potential V at substrate become stability. The results of loop calculation 1000 times (calculation 1000×870 times) simulated in fig.2.5: 1) charge distribution was showed in a); 2) charge intensity at center is lowest, and highest at edge; 3) potential on the circle substrate is similar after loop calculation 1000times.

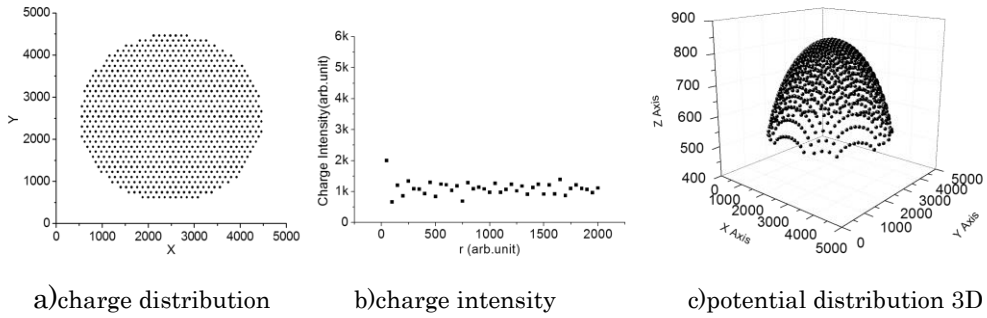


**Fig.2.4 Surface electron distribution and potential distribution. II=0**

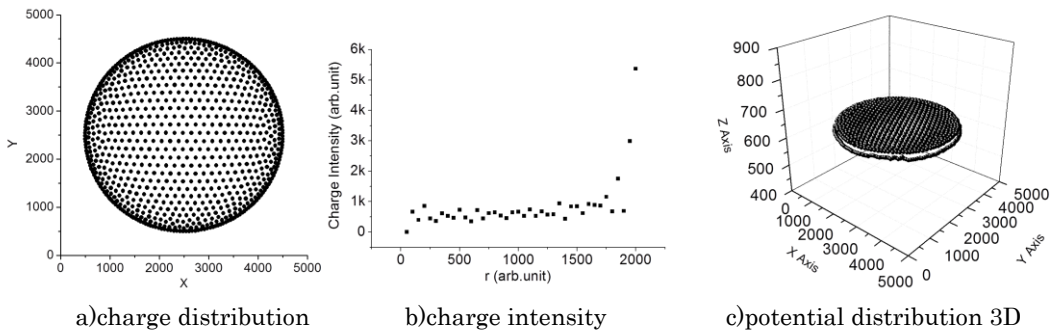


**Fig.2.5 Surface electron distribution and potential distribution. II=1000**

From equations 1-4, excited zinc depends on the electrons that adhered on the substrate. The substrate surface is charged by incident electrons. The electron density  $\sigma(r)$  on the substrate should be:

$$\sigma(r) = \frac{2\epsilon_0 V}{e(R^2 - r^2)^{1/2}} \quad (7)$$

Firstly, the sapphire surface was electrified by incident electrons up to the same magnitude of potential as the anode bias. We know that the bias potential is a fixed number from 0V to 240V. From equation 7, to keep the surface potential constant, the surface electron density must depend on the radius. The electron density at edge area is much higher than at the center, on other hand, distance between electrons at edge area is smaller than at the center. Excited zinc depended on electron intensity, so that excited zinc growth from edge. Furthermore, distance between excited zinc at edge area is smaller than that at the center, because excited zinc depended on electron. From equation 7, the intensity of excited zinc depended on the surface electron intensity. The zinc atoms were deposited on the insulative area.

# *Chapter 3    EXCITED STATE DEPEND ON ENERGY*

## *3.1 The Selection Rule [21] [22]:*

In physics and chemistry, a selection rule, or transition rule, formally constrains the possible transitions of a system from one quantum state to another. Selection rules have been derived for electronic, vibrational, and rotational transitions in molecules. The selection rules may differ according to the technique used to observe the transition.

Transition of electrons by light is a one-photon process caused by the e-photon interaction. Interaction of the one-photon process can be expressed as a sum term of the term of electric dipole transition (E1), the term of magnetic (M1) dipole transitions, and the term of electric quadrupole (E2) transition.

Selection principle of electric dipole transition:

From the of Wigner-Eckart theorem, selection principle obtained as the following:

$$\Delta j = 0, \pm 1$$

$$\Delta m = 0, \pm 1$$

However, in the case such as the following is forbidden, exceptionally.

$$j' = 0 \rightarrow j = 0$$

$$m' = 0 \rightarrow m = 0 (\Delta j = 0)$$

Assuming the LS bond, it becomes selection principle as follows.

$$\Delta L = 0, \pm 1$$

$$\Delta S = 0$$

However, in the case such as the following is forbidden, exceptionally.

$$L' = 0 \rightarrow L = 0$$

And this is called Laborite selection principle, and Spin selection principle.

### 3.2 The Results of XRD

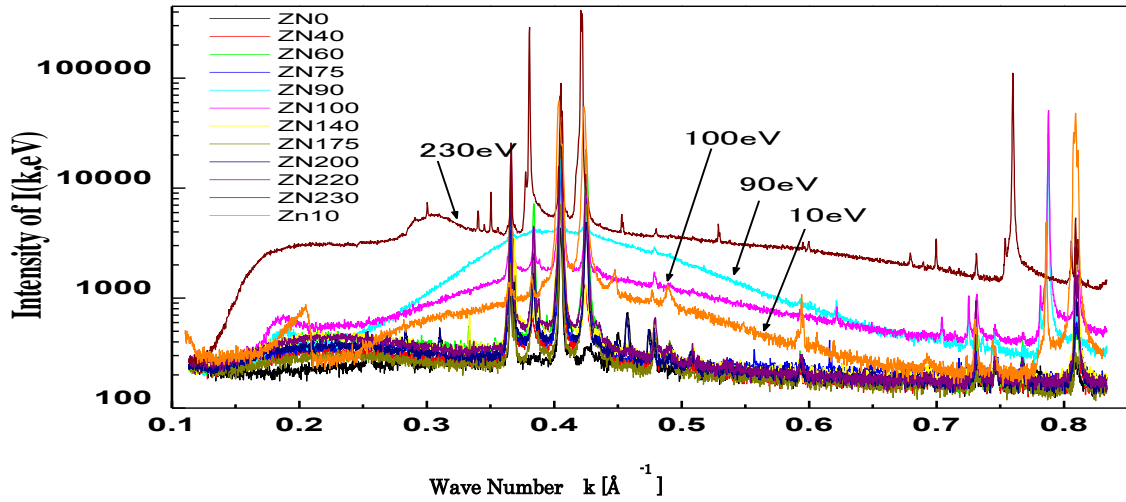


Fig.3.1 Results of XRD from excited zinc condensates. Intensity of diffuse scattering is strong while the incident electron energy equal 10eV, 90eV, 100eV and 230eV. On the other hand, intensity of Bragg diffraction is strong when the incident electron energy equal 10eV, 100eV, 140eV and 230eV. [20]

Table 3.1 The lattice structure of Zn and ZnO [44]

| k<br>( $\text{\AA}^{-1}$ ) | Zn(Hexagonal)       |         | ZnO (Hexagonal)    |         |
|----------------------------|---------------------|---------|--------------------|---------|
|                            | a=2.6575<br>c=4.938 | k       | a=3.250<br>c=5.207 | k       |
| 0.366                      | $K_{\beta}$         |         |                    |         |
| 0.380                      | $K_{\beta}$         |         |                    |         |
| 0.405                      | (0_0_2)             | 0.40502 | (0_1_1)            | 0.40388 |
| 0.421                      |                     |         |                    |         |

Fig.3.1 shows results of XRD from condensates of zinc excited thin films. The bias was exchanged from 0V to 240V, and then the incident electron energy corresponded to 0eV to 240eV. The X-ray diffraction includes Bragg diffraction and diffuse scattering. X-ray diffraction intensities of zinc excited thin films show very strong diffuse scattering at 10eV, 90eV, 100eV and 230eV, while X-ray diffraction intensities show very strong Bragg diffraction at 10eV, 100eV, 140eV and 230eV.

Table 3.1 shows the lattice structure of Zn and ZnO. The wave number  $k$  at  $0.366\text{\AA}^{-1}$ ,  $0.38\text{\AA}^{-1}$  corresponded to  $k_{\beta}$  of hexagonal close-packed structure of zinc and  $0.405\text{\AA}^{-1}$  corresponded to (0-0-2) of zinc, which with the hexagonal close-packed structure. The wave number at  $0.404\text{\AA}^{-1}$  also corresponded to (0-1-1) of zinc oxide, which with the hexagonal close-packed structure.

### ***3.3 Intensity of Diffuse Scattering and Bragg Diffraction Depend on Irradiation Electron Energy***

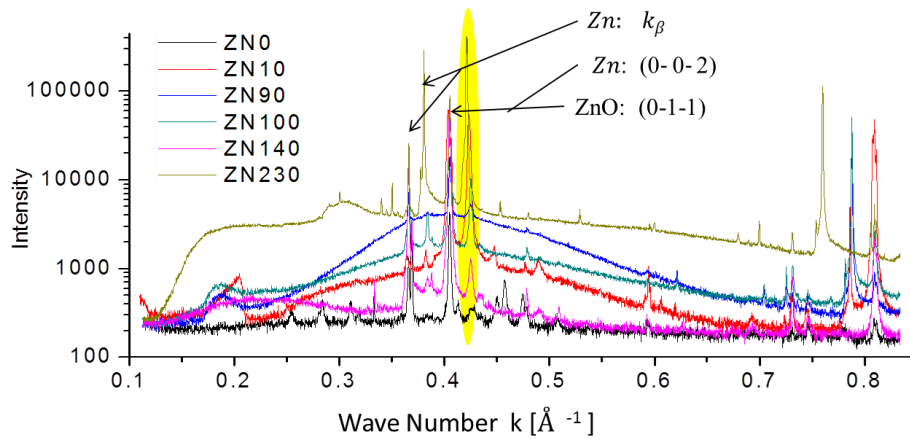


Fig.3.2 shows the results of XRD from zinc excited thin films, while the bias equal 0V, 10V, 90V, 100V, 140V and 230V.

XRD data include diffuse scattering and Bragg diffraction, and it can be written as

$$I(k, eV) = I_{Diffuse}(k, eV) + I_{Bragg}(k, eV)$$

From fig.3.2, X-ray diffraction intensities of zinc excimer thin films shows

very strong diffuse scattering at 10eV, 90eV, 100eV and 230eV, which corresponded to zinc electron binding energy follow  $B.E_{Zn3d}=10eV$ ,  $B.E_{Zn3p}=90eV$ ,  $B.E_{Zn3d+Zn3p}=10eV+100eV$ ,  $B.E_{Zn3p+Zn3s}=90eV+140eV$ . X-ray diffraction intensities of zinc excited thin films shows very strong Bragg diffraction at 10eV, 100eV, 140eV and 230eV, which corresponded to zinc electron binding energy follow  $B.E_{Zn3d}=10eV$ ,  $B.E_{Zn3d+Zn3p}=10eV+100eV$ ,  $B.E_{Zn3s}=140eV$ ,  $B.E_{Zn3p+Zn3s}=90eV+140eV$ . Wave number  $k$  at  $0.366 \text{ \AA}^{-1}$ ,  $0.38 \text{ \AA}^{-1}$  and  $0.405 \text{ \AA}^{-1}$  corresponded to the hexagonal close-packed structure of Zn and ZnO. There isn't zinc compounds corresponded to  $k=0.421 \text{ \AA}^{-1}$ , what means a new zinc structure, perhaps.

### ***Diffuse scattering:***

$$I_{diffuse}(eV) = \int_{k_{min}}^{k_{max}} I_{Diffuse}(k, eV) dk$$

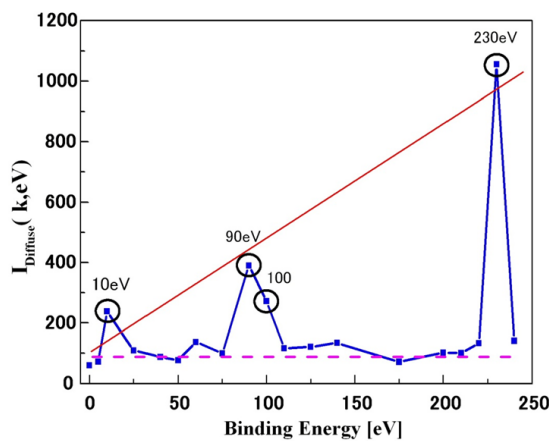


**Fig.3.3 Energy dependence of the diffuse scattering intensity.**

Energy dependence of the integrated intensity of diffuse scattering in fig 3.1 was showed in fig.3.3. The diffuse scattering intensity at 10eV, 90eV, 100eV and 230eV are very strong, but the intensity of diffuse scattering at the other energy could be ignorable. Binding energy of zinc 3d is 10eV, Binding energy of zinc 3p is 90eV, binding energy of zinc 3p plus 3d is 90+10=100eV, and binding energy of zinc 3p plus 3d is 90+140=230eV. Intensity of diffuse scattering is strong when incident energy is equivalent to the zinc binding energy.

***Bragg diffraction:***

$$I_{\text{Bragg}}(k, eV) = \int_{\text{peak}(k=i)} I_{\text{Bragg}}(eV) d_k$$

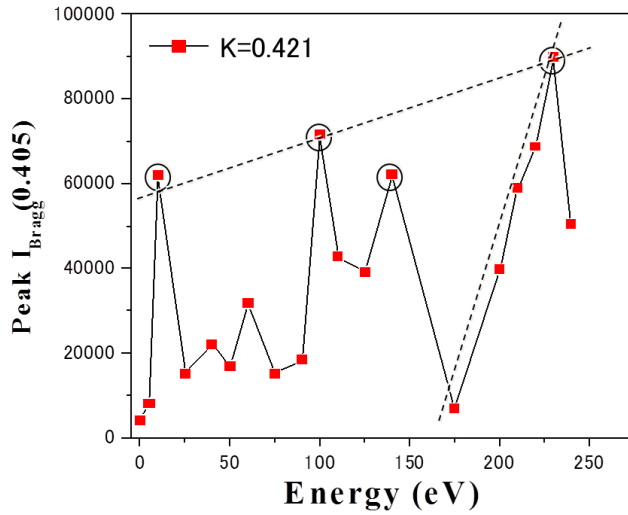


**Fig.3.4 Energy dependence of the Bragg diffraction.**

The fig.3.4 showed integrated intensity of peaks of  $k=0.421$ , what profiles at 10eV, 100eV, 140eV and 230eV broadened as electron energy increased. Then apparent enhancements of diffuse scattering intensities observed at 10eV, 100eV, 140eV, 230eV. The intensities of enhanced peaks were approximately proportional to the energy of incident electron as indicated by the linear increase at 170~230eV. On the other hand, the electron energy dependence of the peak intensities of Bragg reflection is shown as indicated by the linear increase while bias voltage is bigger than 170V.

### 3.4 Energy Dependence and Excited Type of Zinc

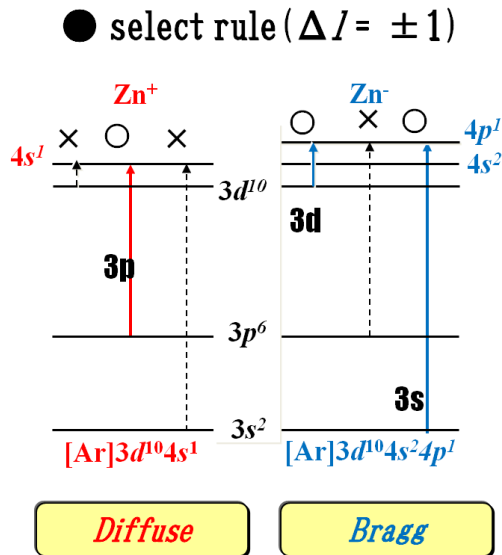


Fig.3.5 Excited type of zinc depended on select rule.

The electron excitation process depends on the initial and the final states in ions. The initial electron states of both ions are [Ar]3d<sup>10</sup>4s<sup>1</sup> for Zn<sup>+</sup>, and [Ar]3d<sup>10</sup>4s<sup>2</sup>4p<sup>1</sup> for Zn<sup>-</sup>. The excitation model from the inner-core electron states to the 4s<sup>1</sup> state for Zn<sup>+</sup>. And 4p<sup>1</sup> state for Zn<sup>-</sup> is shown in fig.3.5. According to selection rule,  $\Delta l = \pm 1$ . The 3d state and 3s state in Zn<sup>-</sup> are possibility of transiting to the 4p state; however in Zn<sup>+</sup>, only the 3p state has possibility of transitioning to the 4s state. So, the diffuse scattering is caused by inner core electron states 3p excited to the 4s state by Zn<sup>+</sup>, however Bragg diffraction is caused by inner core electron states 3s and 3d excited to the 4p state by Zn<sup>-</sup>. It's accordance with the XRD data analyses of section 3.3. In these experiments, double excitations be excited when the bias voltage is 100V or 230V, while incidence electrons has an energy of 100eV (3d+3p) or 230eV (3p+3s). And double excitations were very effective to form excited states with long lifetime ( $\tau > 44$  weeks) what was shown by results of XPS.

### ***3.5 The Properties of Excited Zinc Films***

From figures, discrete dependence between diffuse scattering intensity to electron energy corresponded to inner shell binding energy of zinc atom 3d (10eV), 3p (90eV), 3s (140eV), 3d+3p (10+90=100eV), 3p+3s (90+140=230eV). By the quantum selection rule  $\Delta l = \pm 1$ , 3s and 3d is excitable to 4p of  $Zn^-$ , 3p is excitable to 4s of  $Zn^+$ . 140eV and 90eV showed the different nature of excitation. Excitation of 3p (90eV) from  $Zn^+$  showed a very strong diffuse scattering. Excitation of 3s (140eV) from  $Zn^-$  showed a very strong Bragg diffraction.  $Zn^-$  and  $Zn^+$  were double excitable energy, 230eV, with the fastest generation efficiency.

The samples showed strong diffuse scattering and Bragg diffraction, what divided into crystals and non-crystalline structures, in other hands, the special zinc film should be a polycrystalline or amorphous. It was expected to have movement easy physical properties [23][24].

# *Chapter 4 THE THEORIES*

## *4.1 The Excited State*

In quantum mechanics an excited state of a system (such as an atom, molecule or nucleus) is any quantum state of the system that has a higher energy than the ground state (that is, more energy than the absolute minimum). The temperature of a group of particles is indicative of the level of excitation (with the notable exception of systems that exhibit Negative temperature). The lifetime of a system in an excited state is usually short: spontaneous or induced emission of a quantum of energy (such as a photon or a phonon) usually occurs shortly after the system is promoted to the excited state, returning the system to a state with lower energy (a less excited state or the ground state). This return to a lower energy level is often loosely described as decay and is the inverse of excitation [11].

### *Excitation source:*

The excitation source is electron with bias, 0~240eV. Excited state with an inner hole, and exists of an inner hole means a inner electron be excited. A core electron can be excited in at least five different ways: 1. X-ray absorption; 2. X-ray scattering; 3. Electron scattering; 4. Proton or ion scattering; 5. Electron capture in some isotopes. Our group wants to develop a new concept material, that is Zn\* (excited zinc) with a super long lifetime though an excited process with zinc. The energy of x-ray excitation source can't be adjusted freely; on the other hand, energy of electron excitation source can be adjusted freely by electric field [12]. And binding energy and orbital of zinc showed in fig.2.2. The excitation of core electrons at 1s, 2s and 2p need the high energy of excitation source. And core hole is unstable; it lives for  $\sim 10^{-15}$  seconds before it decays via radioactive or nonradioactive decay channels. Form section 2.1, our purpose is to create super long lifetime zinc 3d hole. To save energy, our excitation source energy set at 0~240eV and 230eV=90eV+140eV, what equal sum binding energy of 3p and 3s of zinc atom.

### *The lifetime of excited states:*

In quantum mechanics, an excited state of a system (such as an atom, molecule or nucleus) is any quantum state of the system that has a higher energy than the ground state (that is, more energy than the absolute minimum). The excited state means inner hole of atoms is created. An atom with a core hole is extremely unstable. The lifetime of the core hole is of the order of  $10^{-15}$ s or 1fs. The lifetime ( $\tau$ ) is linked to the uncertainty in the energy of the core hole ( $\Gamma$ ) via the Heisenberg uncertainty relation [13]:

$$\Gamma\tau \cong \hbar = 10^{-16}\text{eVs}$$

A lifetime of 1 fs implies a lifetime broadening of 0.1eV. There are two major decay processes: fluorescence and Auger. These usually occur shortly after the system is promoted to the excited state, returning the system to a state with lower energy (a less excited state or the ground state). This return to a lower energy level is often loosely described as decay and is the inverse of excitation. Long-lived excited states, on other words, the inner hole has a long lifetime. *The long lifetime excited state of zinc should be a metastable state.* The metastable states like the super cooled state, supersaturated state, glassy state, diamond at room temperature and atmospheric pressure (the most stable graphite), titanium dioxide anatase [14]. And the super long lifetime excited state of zinc should be a glassy state.

## 4.2 Interaction of Polarization Coordination

The research of new material science with zinc was beginning. Exciting zinc is very simple, but how to extend the lifetime of excited zinc atoms is difficult. At first, matter exist like gas, liquid and solid, and the life time of excited state can't be extended in gas phase, so the long lifetime excited zinc must be exist in super cooling liquid phase or solid phase. The excited zinc growth on the sapphire substrate that is stable.

From Fig.4.1, the  $^1\Sigma_g^+$  state formed from two  $^1S$  ground state Zn atoms is essentially repulsive with a shallow van der Waals minimum;  $Zn(^1S)+Zn(^3P)$  would anticipate two bond states and two repulsive states; The singlet states dissociating to  $Zn(^1S)+Zn(^1P)$  should follow a similar pattern:  $^1\Sigma_u^+$  and  $^1\Pi_g$  being attractive and  $^1\Sigma_g^+$  and  $^1\Pi_u$  being repulsive.

The  $^1\Sigma_g^+$  state formed from two  $^1S$  ground states what means potential energy is decreased with the distance of the two  $^1S$  ground states. There is repulsive force between two  $^1S$  grounds.

Fig.4.2 shows on an expanded scal the clearly observable avoided curve crossings in the  $^1\Pi_u$  states. In the figure, the upper end of the vertical arrow shows the true asymptote for infinite separation of  $Zn^+ Zn^-$ . The lower end shows the energy obtained by subtraction  $1/R$  from the asymptote, where the value of  $R$  corresponding to the last computed point has been taken ( $20 a_0$ ). Thus in the figure the two lower states have essentially reached their asymptotic energy at  $20 a_0$  separation, while the upper state would continue to rise 1.36eV in energy. The upper state formed from  $Zn^+(^2S)$  and  $Zn^-(^2P)$  states, what means potential energy is increased with the distance of the two  $^1S$  ground states. There is attracting force between  $Zn^+(^2S)$  and  $Zn^-(^2P)$  ion states.

From the above, ion-recombination can create bound states. And ion is control easily by electric field. In summary, object of long lifetime excited state search is zinc, and the growth process of excited zinc is surface crystal growth process due to ion-recombination.

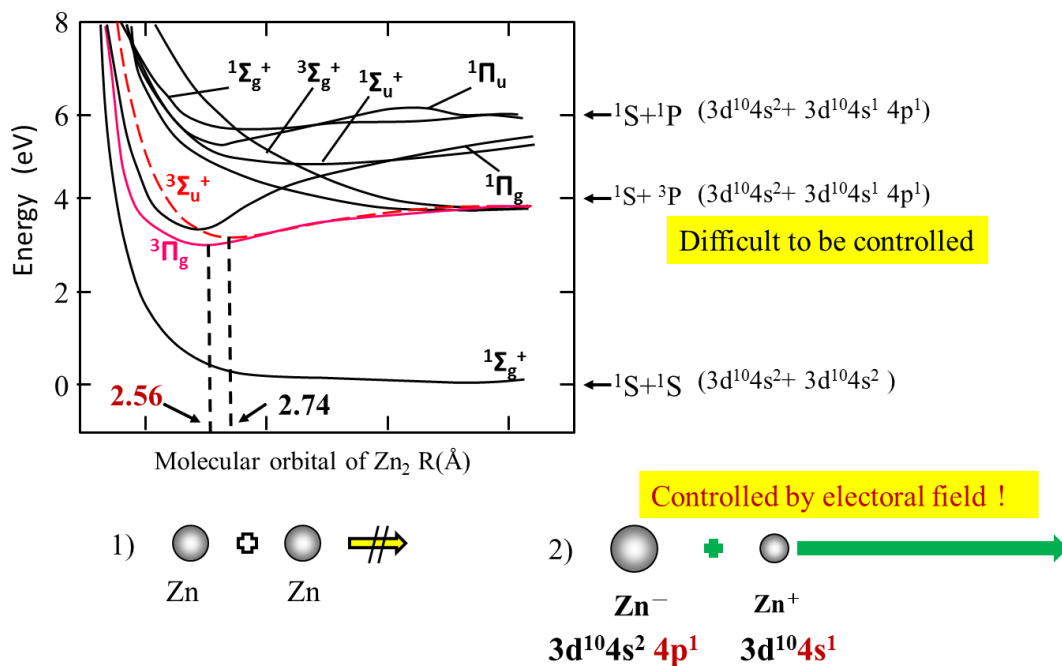


Fig.4.1 Potential energy curves for the states of Zn<sub>2</sub> arising from Zn (<sup>1</sup>S) + Zn (<sup>1</sup>S, <sup>3</sup>P, and <sup>1</sup>P).[15]

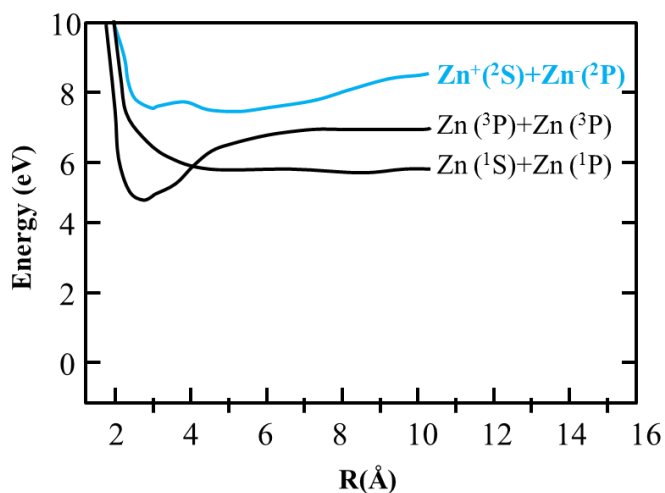


Fig.4.2 Potential energy curves of the <sup>1</sup>Π<sub>u</sub> states of Zn<sub>2</sub> which show the avoided curve crossings with the Zn<sup>+</sup> Zn<sup>-</sup>Π<sub>u</sub> state. [15]

### ***4.3 X-ray Photoelectron Spectroscopy (XPS)***

X-ray photoelectron spectroscopy (XPS) is described with three-step model: at first, absorption of the x-ray, secondly “transport” of the excited photoelectron to the surface, at last, escape of the photoelectron from the surface. In XPS object elements be excited, and the measure is kinetic energy of photoelectron what be excited by absorption x-ray.

#### ***4.3.1 What is X-ray photoelectron spectroscopy?***

X-ray photoelectron spectroscopy (XPS) is a surface-sensitive quantitative spectroscopic technique that measures the elemental composition at the parts per thousand range, empirical formula, chemical state and electronic state of the elements that exist within a material. XPS spectra are obtained by irradiating a material with a beam of X-rays while simultaneously measuring the kinetic energy and number of electrons that escape from the top 0 to 10 nm of the material being analyzed. XPS can be described with the three-step model as shown in Appendix A:

1. Absorption of the X-ray inside the solid.
2. “Transport” of the excited photoelectron to the surface.
3. Escape of the photoelectron from the surface.

In the case of XPS, a core electron is excited by the incident x-ray to the high-energy continuum states and detected as a photoelectron. XPS is first-order optical process that includes only one photon. In the historical development of the study of XPS, the one electron character of XPS was first taken into account, and after that many-body effects were studied. Within the one electron approximation, the kinetic energy of the photoelectron is determined by the energy conservation law as  $E_{\text{kin}} = \hbar\nu - (E_{\text{F}} - E_{\text{c}}) - \phi$  in fig.4.1 where  $\hbar\nu$  is the incident photon energy,  $E_{\text{c}}$  is the core level binding energy,  $E_{\text{F}}$  is Fermi energy, and  $\phi$  is the work function. Theoretically,  $E_{\text{c}}$  is obtained, for instance, by the Hartree-Fock approximation, and then equation represents the Koopmans’ theorem [25].

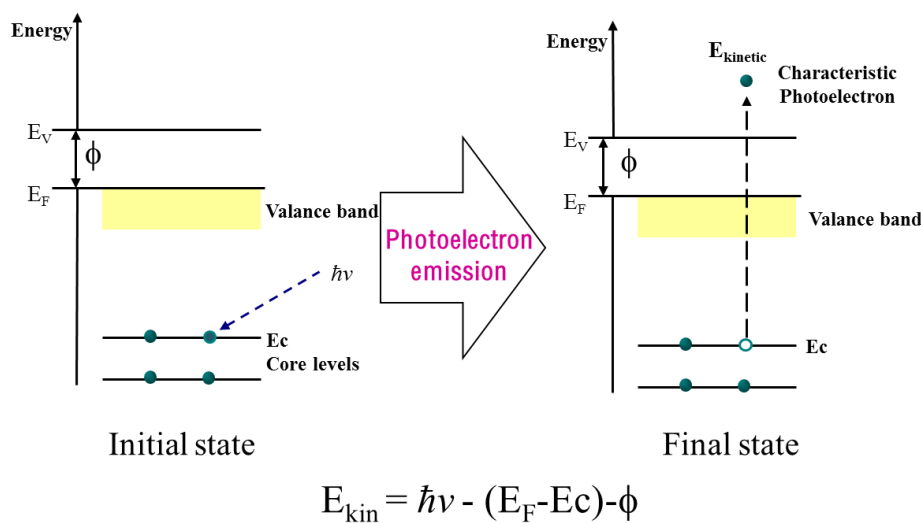


**Fig.4.3 The X-ray photoelectron emission processes**

On the other hand, the value of  $E_c$  can be estimated from the XPS spectrum if the other quantities in this equation are known. Since the value of  $E_c$  is not very much different from the corresponding value of the free atom, which is the characteristic of each element, XPS is useful for the analysis of element in solids. XPS is used to measure: 1) elemental composition of the surface (top 0–10 nm usually); 2) empirical formula of pure materials; 3) elements that contaminate a surface; 4) chemical or electronic state of each element in the surface; 5) uniformity of elemental composition across the top surface (or line profiling or mapping); 6) uniformity of elemental composition as a function of ion beam etching (or depth profiling).

Koopmans' theorem does not generally hold because of the many-body effect beyond the Hartree-Fock approximation [26] [27]. Due to the progress in experimental techniques, the many-body charge-transfer effect in XPS can be observed as an asymmetry of the spectral shape and as satellite structures in various materials. When the core hole is created in the XPS process, VES (the Valence Electron States) are polarized by the core hole potential and screen it. The polarization of VES occurs mainly by the charge transfer effect. Thus, the core hole plays a role of “test charge,” which induced the charge transfer of VES, and the effect of charge transfer is reflected in the XPS spectrum as a spectral asymmetry and satellites.

### 4.3.2 Charge Transfer (CT) in Transition Metal (TM)

Peak that appears in the XPS spectrum except the Auger electron peak and photoelectron peak, collectively referred as the satellite peak. Satellite what means “secondarily” or “subsidiary”. These peaks are roughly classified into the following five categories [27]: A) Satellite peaks derived from the X-ray source; B) Energy loss peak; C) Multiplet splitting peak; D) Shake up, shake off peak; E) Chemical shift. Except these five types of satellite, there is a special satellite peak that origins from charge transfer of transition metal compounds, what with the un-full filled 3d orbital at the ground state.

#### *Charge transfer:*

The photocurrent produced from PES can be obtained from the scattering theory [25][27], which is proportional to the transition probability from Fermi's golden rule expression,

$$J(k, \omega) = \sum_s |\langle N-1, s, k | \Delta | N \rangle|^2 \delta(\hbar\omega - E_k - \varepsilon_s) . . . \quad (8)$$

$E_k$  is the kinetic energy of the photoelectron,  $E_k = \hbar^2 k^2 / 2m$ , and  $\varepsilon_s$  is the excited energy of the remaining solid measured from the initial ground state as  $\varepsilon_s = E(N-1, s) - E(N, 0)$ .  $\hbar\omega$  is the photon energy.  $\Delta$  is the dipole interaction (or optical transition) operator ,

$$\Delta = \sum \langle i | \Delta | j \rangle c_i^\dagger c_j$$

Where  $c_i^\dagger$  and  $c_j$  are the electron creation and annihilation operators, respectively, and  $i$  and  $j$  are the state indices. For the noninteracting case, we have

$$|N-1, s, k\rangle = c_k^\dagger c_s |N\rangle$$

With the index  $s$  for an occupied one-electron state and

$$\langle N-1, s, k | \Delta | N \rangle = \sum_{i,j} \Delta_{i,j} \langle N | c_s^\dagger c_k c_i^\dagger c_j | N \rangle$$

And finally

$$J(k, \omega) = \sum_s |\langle k | \Delta | s \rangle|^2 \delta(\hbar\omega - E_k - \varepsilon_s)$$

$\langle k | \Delta | s \rangle$  Correspond to the dipole matrix element.

To go beyond the non-interacting theory, we return to Eq. (8). Within the sudden approximation, we note

$$\langle N-1, s, k | \Delta | N \rangle = \sum_j \langle N-1, s | \langle k | \Delta | j \rangle c_j | N \rangle$$

And, from Eq. (8),  $J(k, \omega)$  becomes

$$J(k, \omega) = \sum_s \left| \sum_j \langle k | \Delta | j \rangle \langle N-1, s | c_j | N \rangle \right|^2 \times \delta(\hbar\omega - E_k - \varepsilon_s)$$

Defining the single-particle spectral function  $A_{ij}(\varpi)$  as

$$A_{ij}(\varpi) = \sum \langle N-1, s | c_i | N \rangle \langle N | c_j^\dagger | N-1, s \rangle \delta(\varpi + \varepsilon_s)$$

We can re-express  $J(k, \omega)$

$$J(k, \omega) = \sum_{i,j} \langle k | \Delta | i \rangle A_{ij}(E_k - \hbar\omega) \langle j | \Delta | k \rangle$$

It is a common level of approximation to put  $\langle k | \Delta | i \rangle \approx \Delta_k$  and to have

$$J(k, \omega) = |\Delta_k|^2 \sum_{i,j} A_{ij}(E_k - \hbar\omega)$$

In particular, for a core level, i.e.,  $i=j=b$ , without any approximation, we have

$$J(k, \omega) = |\Delta_k|^2 A(E_k - \hbar\omega)$$

With  $\Delta_k = \langle k | \Delta | b \rangle$  and

$$A(\omega) = \sum_s |\langle N-1, s | c_b | N \rangle|^2 \delta(\omega + \varepsilon_s)$$

Here we find that the single-particle spectral function would be a central quantity in understanding the photocurrent by PES. The single-particle spectral function can be calculated by the well-defined and sophisticated mathematical formalism called the single-particle Green's function.

The Fermi golden rule expression for the core-level PES includes the following transition matrix element

$$\langle N-1, k; s | \Delta_{dipole} | N \rangle = \langle N-1; s | \langle k | \Delta_{dipole} | b \rangle | N-1 \rangle$$

In Eq.(1),  $|k\rangle$  is the single-electron state describing the photoelectron and  $|N-1; s\rangle$  is the remaining  $N-1$  electrons in the state  $s$ , while  $|b\rangle$  is the core level under consideration and  $|b\rangle|N-1\rangle$  is the initial ground state before the PES process.  $\Delta_{dipole}$  is the dipole operator. The photocurrent  $J(k, \omega)$  can then be expressed as

$$J(k, \omega) = |\langle k | \Delta_{dipole} | b \rangle|^2 \sum_s |\langle N-1; s | N-1 \rangle|^2 \delta(\omega + \varepsilon_s)$$

There  $\varepsilon_s$  is the binding energy of the excited state measured from the no-loss line. If  $|N-1; 0\rangle \approx |N-1\rangle$ , we have only a peak from  $|\langle N-1; 0 | N-1 \rangle|^2 \approx 1$  for  $s=0$ , and 0 for  $s \neq 0$ . that is, there is no satellite. This case occurs basically only in a no-interacting system, where it is said that the photo hole is completely screened. On the other hand, generally,  $J(k, \omega)$  consists of the core line corresponding to  $|b\rangle$  and its accompanying satellites according to the number of excited states  $s$  in the PES process. It should be also noted that the present argument could be applied not only to the core line but also the valence spectra. In the following subsections, we provide some examples of rather famous satellite problems of the PES and their proper understanding.

### 4.3.3 Hund's rules and final state effects of atomic multiplets

The ground states symmetries of the TM compounds, which are characterized with a partly-filled 3d band. The term symbols with the lowest energy are found after calculation the matrix elements, following the rules as described previously. Finding the  $^3F$  state as the ground state of a  $3d^2$  configuration is an example of Hund's rules [28][29]. On the basis of experimental information, Hund formulated three rules to determine the ground state of a  $3d^n$  configuration. For  $3d^n$  configurations, the rules are correct, as confirmed by the atomic multiplet calculations. The three rules are:

1. Term symbol with maximum S.
2. Term symbol with maximum L.
3. Term symbol with maximum J (if the shell is more than half-full).

The 2p x-ray absorption process excites a 2p core electron into the empty 3d shell and the transition can be described as  $2p^63d^0 \rightarrow 2p^53d^1$ . The  $2p^53d^1$  configuration contains two new terms in its Hamiltonian: the 2p spin-orbit coupling and 2p3d multiplet effects [30]. The final state atomic energy matrix consists of terms related to the two-electron Slater integrals ( $H_{\text{electro}}$ ) and the spin-orbit couplings of the 2p ( $H_{\text{LS-2p}}$ ) and the 3d electrons ( $H_{\text{LS-3d}}$ ):

$$H_{\text{eff}} = H_{\text{electro}} + H_{\text{LS-2p}} + H_{\text{LS-3d}} ,$$

$$H_{\text{electro}} = \langle 2p^53d^1 | \frac{e^2}{r_{12}} | 2p^53d^1 \rangle ,$$

$$H_{\text{LS-2p}} = \langle 2p | \zeta_p l_p \cdot s_p | 2p \rangle ,$$

$$H_{\text{LS-3d}} = \langle 3d | \zeta_d l_d \cdot s_d | 3d \rangle .$$

To show the individual effects of these interactions, each will now be introduced separately. A series of five calculations are shown, in which:

1. All final state interactions are set to zero:  $H=0$
2. 2p spin-orbit coupling is included:  $H=H_{\text{LS-2p}}$
3. Slater-Condon parameters are included:  $H=H_{\text{electro}}$

4. 2p spin-orbit coupling and Slater-Condon parameters are included:

$$H=H_{\text{electro}}+H_{\text{LS-2p}}$$

5. 3d spin-orbit coupling is included:  $H=H_{\text{electro}}+H_{\text{LS-2p}}+H_{\text{LS-3d}}$

#### 4.3.4 Initial state and final state of TM[31][32]

Here, we discuss the analysis of 2p XPS of TM (Transition Metal) compounds by CTM (Charge Transfer Multiplet) calculations with cluster models, taking into account two configurations  $3d^n$  and  $3d^{n+1}\underline{L}$  for  $\text{Cu}^{2+}$  compound and three configurations,  $3d^n$ ,  $3d^{n+1}\underline{L}$  and  $3d^{n+2}\underline{L}^2$  for other compound. The Hamiltonian, which includes the TM 2p core states explicitly so that it is applicable to both initial and final states of XPS, is given by

$$\begin{aligned} H = & \sum_{\nu} \varepsilon_{\Gamma} \alpha_{\nu}^{\dagger} \alpha_{\nu} + \sum_{\nu} \varepsilon_{d\Gamma} \alpha_{d\nu}^{\dagger} \alpha_{d\nu} + \sum_{\mu} \varepsilon_{2p} \alpha_{p\mu}^{\dagger} \alpha_{p\mu} + \sum_{\nu} V(\Gamma) (\alpha_{d\nu}^{\dagger} \alpha_{\nu} + \alpha_{\nu}^{\dagger} \alpha_{d\nu}) \\ & + \frac{1}{2} \sum_{\nu_1, \nu_2, \nu_3, \nu_4} g_{dd}(\nu_1, \nu_2, \nu_3, \nu_4) a_{d\nu_1}^{\dagger} a_{d\nu_2} a_{d\nu_3}^{\dagger} a_{d\nu_4} \\ & + \sum_{\nu_1, \nu_2, \mu_1, \mu_2} g_{pd}(\nu_1, \nu_2, \mu_1, \mu_2) a_{d\nu_1}^{\dagger} a_{d\nu_2} a_{p\mu_1}^{\dagger} a_{p\mu_2} \\ & + \zeta_d \sum_{\nu_1, \nu_2} (1 \cdot s)_{\nu_1 \nu_2} a_{d\nu_1}^{\dagger} a_{d\nu_2} + \zeta_p \sum_{\mu_1, \mu_2} (1 \cdot s)_{\mu_1 \mu_2} a_{p\mu_1}^{\dagger} a_{p\mu_2} \end{aligned}$$

Here  $\nu$  denotes the combined indices ( $\Gamma, \sigma$ ),  $\mu$  is similar indices for the 2p core level (so that  $\Gamma$  is replaced by an atomic orbital angular momentum),  $g_{dd}$  and  $g_{pd}$  represent the Coulomb interaction between 3d states and that between 2p and 3d states, respectively, and  $\zeta_d$  and  $\zeta_p$  are the spin-orbit coupling parameters. It is to be noted that  $g_{dd}$  and  $g_{pd}$  include not only the spherical symmetric components,  $U_{dd}$  and  $U_{dc}$ , but also the multi-pole components, which include the Slater integrals in their explicit forms. The Slater integrals,  $F^2(3d, 3d)$ ,  $F^4(3d, 3d)$ ,  $F^2(2p, 3d)$ ,  $G^1(2p, 3d)$ ,  $G^3(2p, 3d)$ , and the spin-orbit coupling parameters  $\zeta_d$  and  $\zeta_p$  are calculated by an atomic Hartree-Fock program, and then the Slater integrals are scaled down to 85%.

Factors of charge transfer energy ( $\Delta$ ), mixing energy (T) and coulomb interaction energy between 3d ( $U_{dd}$ ) and inner holes (Q or  $U_{dc}$ ) are the most

important factors in charge transfer process. The charge-transfer energy  $\Delta$  is now redefined by

$$\Delta \equiv E[3d^{n+1}\underline{L}] - E[3d^n],$$

Where  $E[3d^{n+1}\underline{L}]$  and  $E[3d^n]$  represent the configuration averaged energies of  $3d^{n+1}\underline{L}$  and  $3d^n$ , respectively. Then we have the following relations:

$$\Delta + U_{dd} = E[3d^{n+2}\underline{L}^2] - E[3d^{n+1}\underline{L}],$$

$$\Delta - U_{dc} = E[2p^5 3d^{n+1}\underline{L}] - E[2p^5 3d^n],$$

$$\Delta + U_{dd} - U_{dc} = E[2p^5 3d^{n+2}\underline{L}^2] - E[2p^5 3d^{n+1}\underline{L}],$$

In fig.4.4, we show an ionic state energy diagram of XPS. Here we consider the Ni 2p XPS process of a divalent Ni compound, where we assume that  $\Delta = 4\text{eV}$ ,  $U_{dd} = 8.5\text{eV}$ . The two curves represent the energies of ground state configurations and final state configurations. If the energy of the  $3d^8$  configuration (3d count = 8) in the ground state is taken as the origin of the energy, then that of the  $3d^9\underline{L}$  (3d count = 9) is  $\Delta$ . If we take the energy of the  $3d^8$  configuration in the final state as  $E_0$ , the energy of  $3d^9\underline{L}$  is  $E_0 + \Delta - U_{dc}$ . In fig.4.4,  $E_0$  is taken to be  $10\text{eV}$  (the offset energy). The energy of the  $3d^{10}\underline{L}^2$  configuration (3d count = 10) is  $2\Delta + U_{dd}$  for the ground state and  $E_0 + 2\Delta + U_{dd} - 2U_{dc}$  for the final state. Going in the opposite direction, the energy of  $3d^7\underline{L}$  is equal to  $-\Delta + U_{dd}$  for the ground state and  $E_0 - \Delta + U_{dd} + U_{dc}$  for final state, where the energy difference of L (ligand electron) and  $\underline{L}$  (ligand hole) is neglected for simplicity. This figure is based on the work of John Fuggle who introduced this figure for VPES spectra of RE systems (Fulle et al., 1983). The arrows indicate the XPS transitions in which a 2p core electron is excited to an empty state. This implies the transition from  $3d^8$  to  $2p^5 3d^8$  and so on. The energy of  $2p^5 3d^9\underline{L}$  is lower than that of  $2p^5 3d^8$ , which means that the ionic configuration at the lowest energy is dominated by the  $2p^5 3d^9\underline{L}$  configuration (i.e. the well screened state).

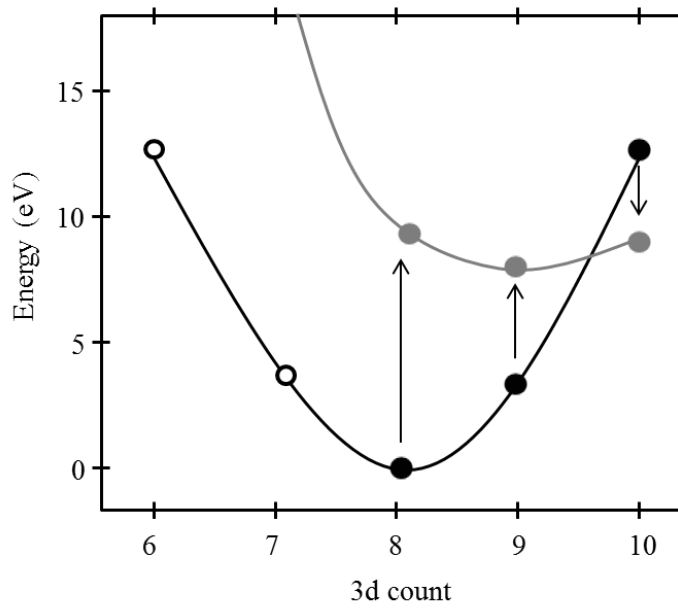


**Fig.4.4** The energy effects in a 2p XPS experiment of a Ni<sup>2+</sup> ion. The dark curve describes the ground state (Initial State). The light curve is the 2p XPS spectrum offset by 10eV. The arrows indicate the 2p XPS transitions (Final State). [33]

#### *4.4 The 2p XPS of TM*

From fig.4.5, all of the transition metal fluorides are with the satellites at high binding energy side, except  $\text{ZnF}_2$ . Intensity of satellite dependent on the ions of transition metal. The distance between main peak is 6eV, be fixed.

Here we consider the 2p XPS of the TM difluoride series from  $\text{ZnF}_2$  to  $\text{MnF}_2$ . The dots are experimental data observed by Rosencwaig et al. (1971). There is no satellite peak in the Zn 2p XPS of  $\text{ZnF}_2$  where the 3d shell is full filled. However, for  $\text{CuF}_2$ , a strong satellite occurs on the higher binding energy side of the main peak. The intensity of the satellite peak decreases in going from  $\text{CuF}_2$  to  $\text{MnF}_2$ . For  $\text{NiF}_2$ ,  $\text{NiO}$ ,  $\text{NiCl}_2$  and  $\text{NiBr}_2$ , the strong satellites occurred on the higher binding energy side of the main peak. The distance between the satellite peak and main peak increased in going from  $\text{NiF}_2$  to  $\text{NiBr}_2$ .

This satellite was first considered to be caused by the shake-up transition between the metal 3d and 4s orbital, but it is now well established that it originates from the charge transfer between the ligand and metal 3d orbital. The theoretical analysis of such a satellite structure has been successfully made using the cluster model.

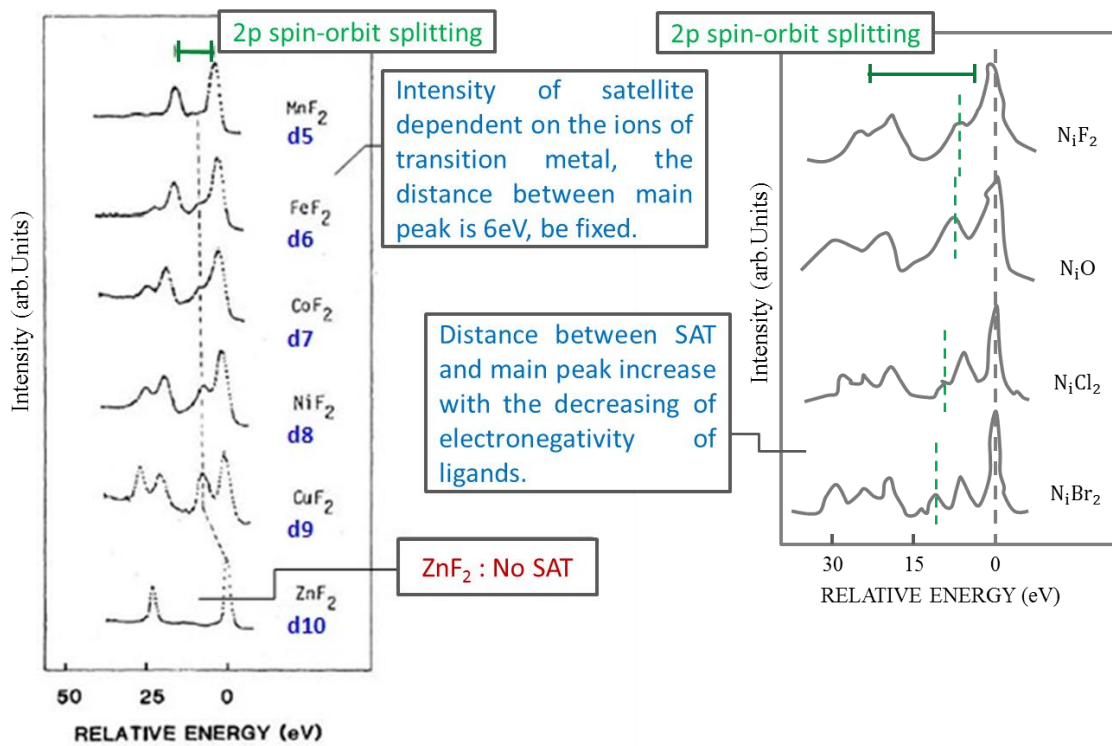


Fig.4.5 2p XPS of transition metal. [31] [37]

## 4.5 Charge Transfer in TM (CuO and Cu)

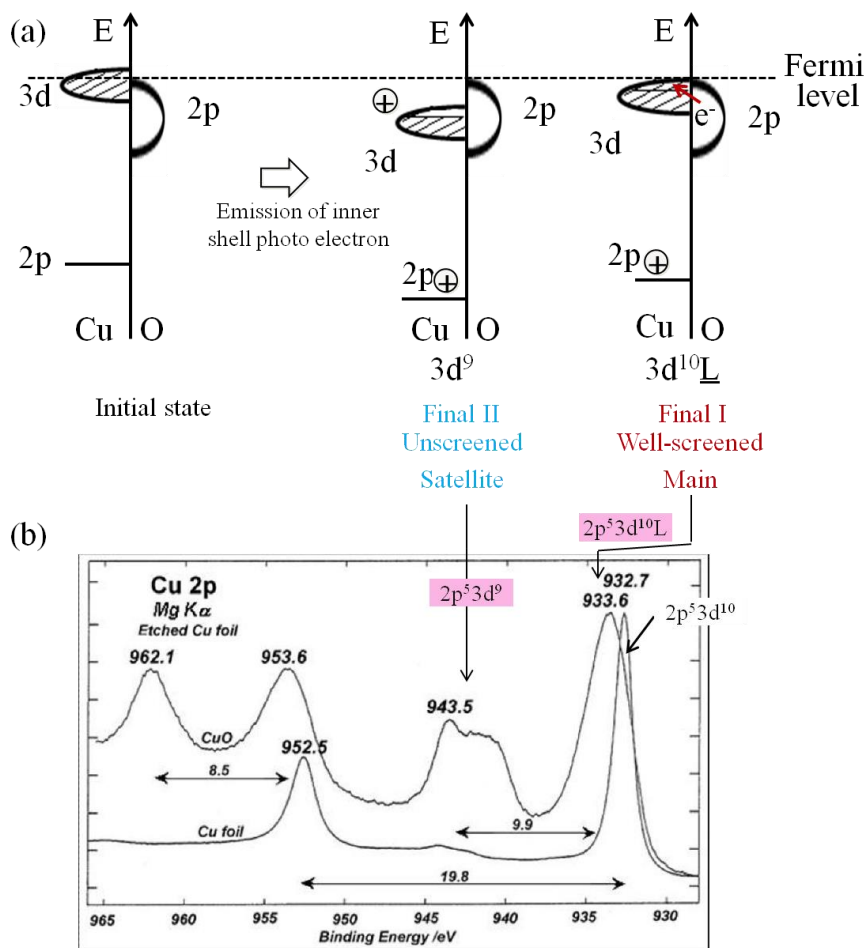


Fig.4.6 The example of satellite by charge transfers; (a) The initial state and final state of CuO; (b) The spectrum of CuO and Cu. [34][35]

We introduce the spectrum of Cu 2p XPS of CuO and Cu. Firstly, the Cu 2p peak of XPS is split to  $2p_{3/2}$  and  $2p_{1/2}$ , and due to the spin-orbit coupling. Incidentally, each of two lines ( $2p_{3/2}$  and  $2p_{1/2}$ ) is further split to the main line (lower binding energy side) and satellite (higher binding energy side). In the ground states of CuO,  $\text{Cu}^{2+}$  has one hole in the 3d shell and the ligand oxygen 2p shell is 6 completely filled. This is usually written as  $3d^9L$ , where  $3d^9$  refers to  $\text{Cu}^{2+}$  and L refers to the outer full filled ligand, oxygen.

To copper foil, because of the full filled 3d, charge transfer hasn't occur before and after the photoelectron emission. The orbital electron could be written as  $2p^63d^{10} \rightarrow 2p^53d^{10}$ . There is a photo-hole in the core-level after photoelectron emission. In the XPS spectra, shake peak at the lower binding energy side is  $2p^53d^{10}$ .

To CuO, there are two final states after the core-hole creation. Final I, in a well-screen condition, one electron transfer from the ligand O 2p to the Cu 3d; the orbital electron could be written as  $2p^63d^9 \rightarrow 2p^5d^{10}L$ . In XPS, it corresponds to the main line. Final II, in an un-screen condition, the charge transfer haven't happened, and the orbital electron could be written as  $2p^63d^9 \rightarrow 2p^5d^9$ .  $2p^53d^9$  corresponds to the satellite at the high binding energy side, as inscribed in fig. 4.6.

This can be understood by considering the additional Coulomb attraction  $Q$  between the core hole and the 3d shell electron. A photo-hole on the metal ion acts as a positive charge for electrons with orbital radius larger than that of the shell on which the photo-hole resides. This lowers the energy of the 3d valence shell by pulling it down below the top of the ligand valence band. This picture neglects the infinite nature of a solid, but could be applied to open d or f shell ions with the localized nature of the orbital by Kotani and Toyozawa [35]. For a rigorous understanding, the theoretical calculation of the band structure for one-hole final state may be necessary, but it would not be easy. Instead, owing to the local nature, much simpler model with a single metal ion and the ligand cluster surrounding the metal ion is available. This approach using the molecular-orbital model was first taken by Asada and Sugano.

There are similar 2p XPS spectra of transition metals. There are satellites at the high binding energy side of the main peaks. The satellites caused by 3d hole. But the satellite of Zn 2p never is reported in other papers. If we can detect out satellites of Zn 2p XPS, 3d hole of zinc is proofed. That means inner shell is excited.

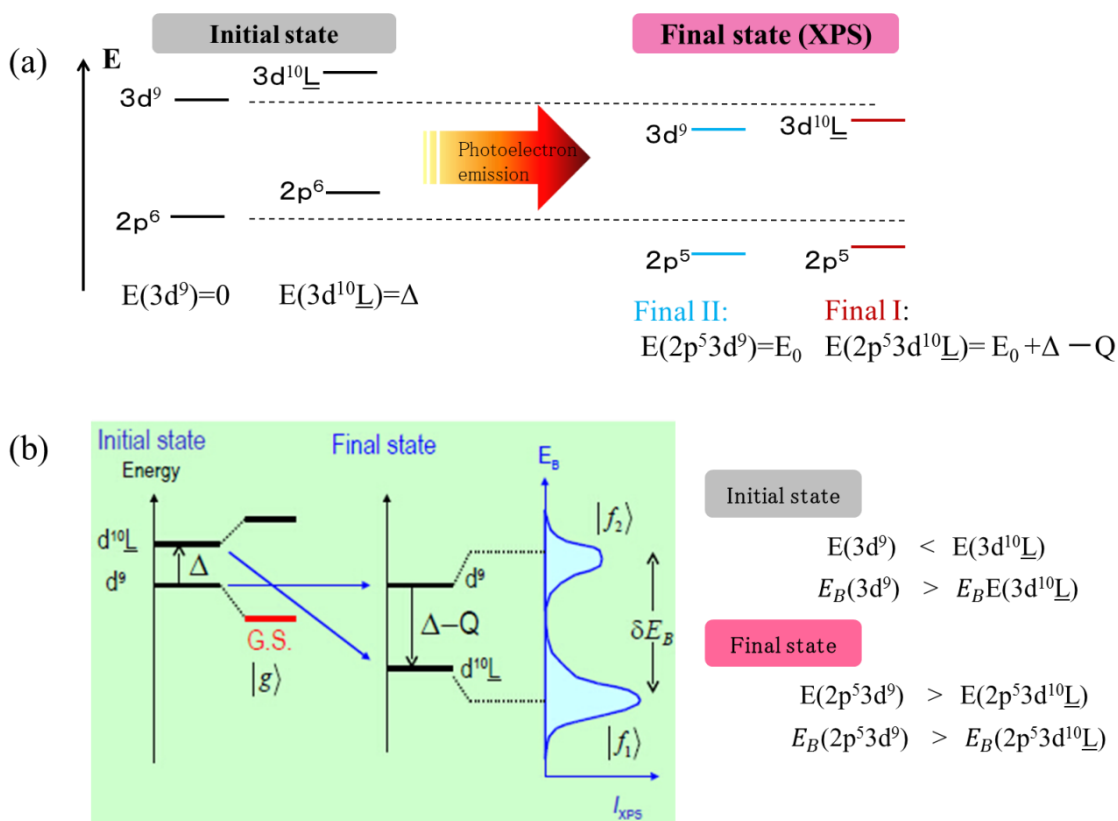


Fig.4.7a The energies of initial states and final states; Fig.4.7b The relationships between final state and XPS spectra. ( $\Delta < Q$ )

Consider the energy of initial state  $3d^9$  is 0. The energy of initial state,  $3d^{10}\underline{L}$  equal  $0+\Delta$ . Binding energy of  $3d^{10}\underline{L}$  is smaller than  $3d^9$ . In final state, consider the energy final state of  $2p^5 3d^9$  is  $E_0$ . The energy of final state  $2p^5 3d^{10}\underline{L}$  equal  $E_0+\Delta-Q$ . To  $2p^5 3d^{10}\underline{L}$ , one electron transfer from the ligand O2p to the Cu3d, charge transfer energy,  $\Delta$ , increased. And there is coulomb gravitational interaction between 2p-hole and 3d-electron,  $Q$ , so, energy of  $2p^5 3d^{10}\underline{L}$  decreased  $Q$ . The energy of  $2p^5 3d^{10}\underline{L}$  is smaller than  $2p^5 3d^9$ . Refer to equivalent core model (ECM); the binding energy of final state is increase than initial state. And binding energy of 2p<sup>5</sup> at  $2p^5 3d^{10}\underline{L}$  decrease than 2p<sup>5</sup> of  $2p^5 3d^9$ , because of there is an electron at 3d orbital of  $2p^5 3d^{10}\underline{L}$  more than  $2p^5 3d^9$ . Finally, binding energy of  $2p^5 3d^{10}\underline{L}$  is smaller than  $2p^5 3d^9$ . We exhibit in fig.4.7b.

## 4.6 Theoretical Calculations of the Charge Transfer

### Parameters

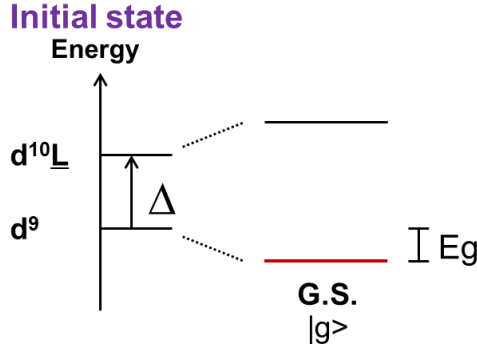


Fig.4.8. Energy of initial state and ground state about charge transfer.

Based on the theories about CT in chapter 4, theoretical calculations of the charge transfer parameters about Configuration-Interaction (CI) Approach, basis wave-functions as  $\psi(d^9)$ , and many-body states interaction as  $\psi(d^{10}\underline{L})$  showed in this section.[35][36]

The initial state and final state of the wave-function of  $\psi(d^9)$  and  $\psi(d^{10}\underline{L})$  can be written as:

$$\text{Initial state (Ground state): } |g\rangle = \cos\theta_g |d^9\rangle - \sin\theta_g |d^{10}\underline{L}\rangle$$

$$\text{Final state: } |f_i\rangle = \cos\theta_{f_i} |d^9\rangle - \sin\theta_{f_i} |d^{10}\underline{L}\rangle \quad (i=1,2,3,\dots)$$

The photoemission intensity of XPS is written as:

$$I_{\text{XPS}}(\omega) = \sum_i |\langle f_i | c | g \rangle|^2 \delta(\omega - E_{f_i} + E_g)$$

The Hamiltonian of  $d^9$  and  $d^{10}\underline{L}$  is written as, respectively:

$$\langle d^9 | H | d^9 \rangle \equiv E[d^9] = 9\epsilon_d + \frac{9 \cdot 8}{2} U + \sum_{\text{all}} \epsilon_p$$

$$\langle d^{10}\underline{L} | H | d^{10}\underline{L} \rangle \equiv E[d^{10}\underline{L}] = 10\epsilon_d + \frac{10 \cdot 9}{2} U + (\sum_{\text{all}} \epsilon_p) - \epsilon_p$$

$$\text{Charge-transfer energy: } \Delta \equiv E[d^{10}\underline{L}] - E[d^9] = \epsilon_d - \epsilon_p + 9U$$

The Hamiltonian of  $d^9$  and  $d^{10}\underline{L}$  is written as:

$$H = \begin{pmatrix} E[d^9] & T \\ T & E[d^{10}\underline{L}] \end{pmatrix} \begin{matrix} d^9 \\ d^{10}\underline{L} \end{matrix}$$

Energy of  $E[d^9]$  is shifted to 0eV. The Hamiltonian of  $d^9$  and  $d^{10}\underline{L}$  is rewritten as:

$$(\text{energy origin shift}) \rightarrow H = \begin{pmatrix} 0 & T \\ T & \Delta \end{pmatrix}$$

$$\text{Basis vector: } |d^9\rangle = \begin{pmatrix} 1 \\ 0 \end{pmatrix} \quad |d^{10}\underline{L}\rangle = \begin{pmatrix} 0 \\ 1 \end{pmatrix}$$

$$\text{Ground state vector: } |g\rangle = \cos\theta_g |d^9\rangle - \sin\theta_g |d^{10}\underline{L}\rangle$$

$$\text{Eigenvalue equation: } H|\Psi\rangle = E|\Psi\rangle \quad \begin{pmatrix} 0 & T \\ T & \Delta \end{pmatrix} \begin{pmatrix} \cos\theta \\ -\sin\theta \end{pmatrix} = E \begin{pmatrix} \cos\theta \\ -\sin\theta \end{pmatrix}$$

$$\begin{pmatrix} -E & T \\ T & \Delta - E \end{pmatrix} \begin{pmatrix} \cos\theta \\ -\sin\theta \end{pmatrix} = 0$$

$$\begin{vmatrix} -E & T \\ T & \Delta - E \end{vmatrix} = 0$$

$$E(E - \Delta) - T^2 = 0$$

$$E = \frac{\Delta \pm \sqrt{\Delta^2 + 4T^2}}{2}$$

$$\text{Ground state energy: } E_g = \frac{\Delta - \sqrt{\Delta^2 + 4T^2}}{2}$$

$$\text{Eigenvector: } H|g\rangle = E_g|g\rangle \quad \begin{pmatrix} 0 & T \\ T & \Delta \end{pmatrix} \begin{pmatrix} \cos\theta_g \\ -\sin\theta_g \end{pmatrix} = E_g \begin{pmatrix} \cos\theta_g \\ -\sin\theta_g \end{pmatrix}$$

$$-T\sin\theta_g = E_g \cos\theta_g$$

$$\tan\theta_g = \frac{-E_g}{T} = \frac{\sqrt{\Delta^2 + 4T^2} - \Delta}{2T}$$

$$\cos\theta_g = \frac{T}{\sqrt{E_g^2 + T^2}} \quad \sin\theta_g = \frac{-E_g}{\sqrt{E_g^2 + T^2}}$$

**Theoretical calculation:**

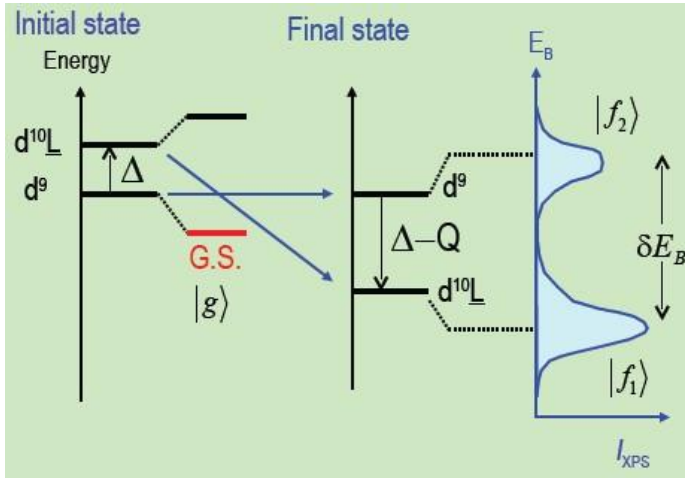


**Fig.4.9** The correspondence between initial state, final state and XPS spectrum of charge transfer process.

The correspondence between initial state, final state and XPS spectrum of charge transfer process was showed in fig.4.9. Factors of  $\Delta$ ,  $T$ ,  $Q$  and  $U_{dd}$  are the most important factors in charge transfer process. In fig.4.6, we show an ionic state energy diagram of XPS. From charge transfer theory by A. Kotani and K. Okada, there is initial state of  $d^9$  and  $d^{10}\underline{L}$ , and energy of  $d^{10}\underline{L}$  state is  $\Delta$  bigger than  $d^9$  state. Mixed valence state of  $d^9$  is marked as “G.S.”, and energy is smaller than  $d^9$  of initial state. The final state originated to emission of inner core electroscopes. If energy of  $\underline{c}d^9 = E_0$ , energy of  $\underline{c}d^{10}\underline{L}$  equal  $E_0 + \Delta - Q$ . About  $T$ ,  $\Delta$ ,  $U_{dd}$  and  $Q$ , the following series of equations is established:

1) Ground state and final state showed as following:

$$\text{G.S. } |g\rangle = \cos\theta_g |d^9\rangle - \sin\theta_g |d^{10}\underline{L}\rangle \quad \tan\theta_g = \frac{E_g}{T} = \frac{\sqrt{\Delta^2 + 4T^2} - \Delta}{2T} \quad (1)$$

$$\text{F.S. } \begin{cases} |f_1\rangle = \cos\theta_f |d^9\rangle - \sin\theta_f |d^{10}\underline{L}\rangle \\ |f_2\rangle = \cos\theta_f |d^9\rangle + \sin\theta_f |d^{10}\underline{L}\rangle \end{cases} \quad \begin{cases} \tan\theta_f = \frac{\sqrt{\Delta_f^2 + 4T^2} - \Delta_f}{2T} \\ \Delta_f = \Delta - Q \end{cases} \quad (2)$$

Photoemission intensity:

$$\begin{aligned} I_{\text{XPS}}(\omega) &= \sum_i |\langle f_i | c | g \rangle|^2 \delta(\omega - E_{f_i} + E_g) \\ &= |\langle f_1 | g \rangle|^2 \delta(\omega - E_{f_1} + E_g) + |\langle f_2 | g \rangle|^2 \delta(\omega - E_{f_2} + E_g) \\ &= \cos^2(\theta_f - \theta_g) \delta(\omega - E_{f_1} + E_g) + \sin^2(\theta_f - \theta_g) \delta(\omega - E_{f_2} + E_g) \end{aligned}$$

2) The peak state energy of  $f_1$  and  $f_2$ , peak interval of  $\delta E_B$ , the intensity ratio of peaks showed as:

$$\text{Final state energy: } E_{f_{1,2}} = \frac{\Delta_f \pm \sqrt{\Delta_f^2 + 4T^2}}{2} \quad (3)$$

$$\text{Peak interval: } \delta E_B \equiv E_{f_2} - E_{f_1} = \sqrt{\Delta_f^2 + 4T^2} \quad (4)$$

$$\text{Intensity ratio: } R = \frac{I_{f_2}}{I_{f_1}} = \tan^2(\theta_f - \theta_g) \quad (5)$$

## *Chapter 5 THE PROOF OF EXCITED ZINC BY XPS*

The sample was deposited at 100°C and 230eV. We discussed experimental results of XPS measurements of center in the sample with 6.5mm; measurements 9 points from N1 to N9, along vertical and horizontal direction in fig.5.1. In this paper, we report the experimental results at vertical. In chapter 6, we measurements 192 points of this sample after 50days. The direction of the incident electron for the surface bias and zinc ionization is parallel to the horizontal direction. Zinc films could conclude Zn what is the reaching object element, Al (substrate of the special excited zinc film is constituted by sapphire, Al<sub>2</sub>O<sub>3</sub>), Si (the effusion cell is constituted by SiO<sub>2</sub>), C (adsorption from environment) and O (Al<sub>2</sub>O<sub>3</sub>, SiO<sub>2</sub> and adsorption from environment). The standard point of binding energy is from Au4f<sub>7/2</sub>(84.0eV), Au<sub>5/2</sub>(87.7eV) and C1s (285.0eV).

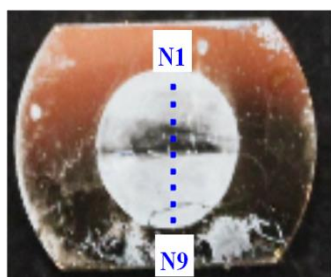


**Fig.5.1 N1-N9 points along vertical, and N5 at the center of sample.**

## 5.1 The XPS Result of 9 vertical points at the center of “Sample 100”

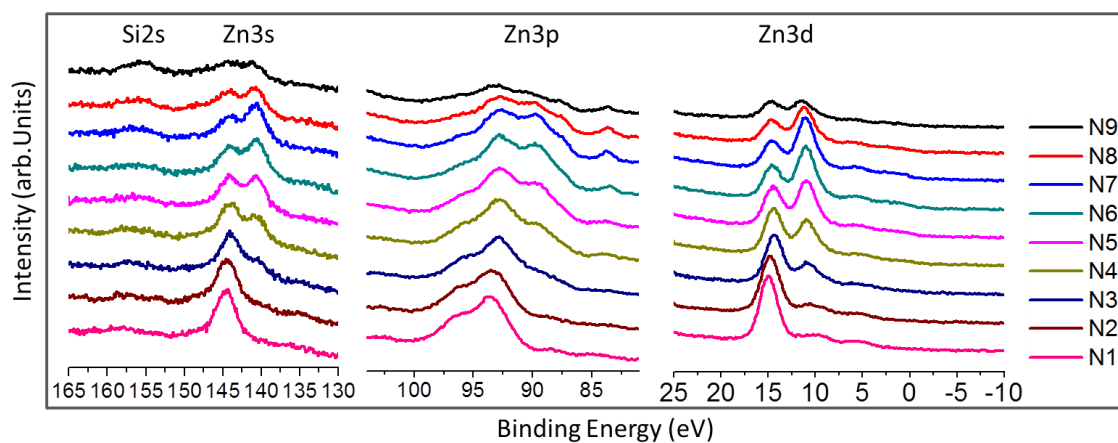


Fig.5.2a The XPS spectrum of Si2s, Zn3s, Zn3p and Zn3d

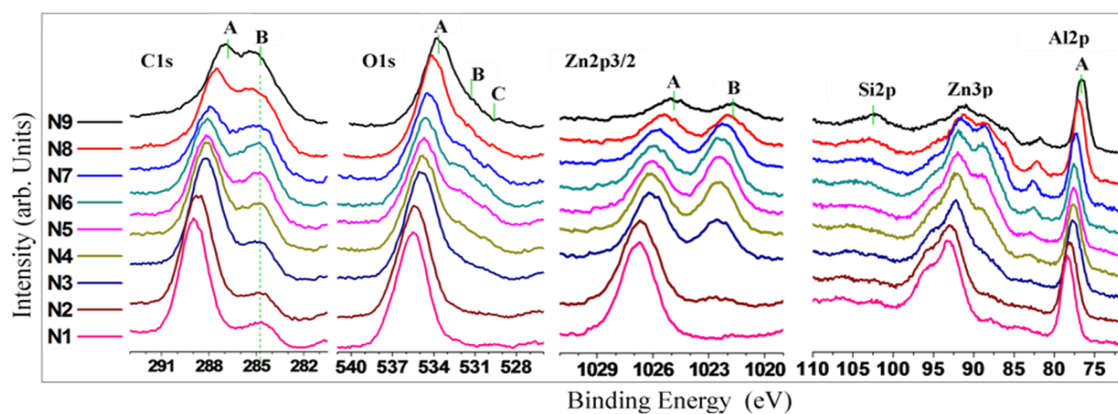


Fig.5.2b The XPS spectrum of C1s, O1s, Zn2p<sub>3/2</sub>, Al2p and Si2p

Fig.5.2 The XPS spectrum of sample after 308days from N1 to N9, and N5 at the center of sample.

Fig.5.1 showed measurement points on the etched zinc film surface. The results of spatial distribution of XPS spectra of Zn3s, Zn3p, Zn3d, C1s, O1s, Zn2p<sub>3/2</sub>, Al2p, Zn3p, Si2s, and Si2p were showed in fig.5.2: C1s spectra, two peaks are recognized, and the separation energy between the two peaks depends on the location. O1s peak profiles are relatively wide, which were fitted by three peaks. There are small shift between peaks of Zn3s, Zn3p, and Zn3d from N1 to N9 in fig.5.2a to the peaks of Zn2p in fig.5.2b. Zn2p<sub>3/2</sub> profiles include two peaks. Intensity of peaks depended on the location, and the two peaks had different dependence on the location. The peaks of B at Zn2p<sub>3/2</sub> mostly exist at the center region of the substrate. Peaks of Zn3p include Zn3p<sub>3/2</sub>, Zn3p<sub>1/2</sub> and shift peaks of Zn3p<sub>3/2</sub> and Zn3p<sub>1/2</sub>. It is difficult to fit out four peaks of those, clearly. Analysis of element, Zinc, is focused on Zn2p<sub>3/2</sub>. The peaks of Si2p spectra almost can't exhibit clearly. Al2p spectra showed strong broad single peak. From the viewpoint of correlation, spectra of C1s at peak A and peak A of Zn2p<sub>3/2</sub> suggest high correlation. And O1s and Al2p also suggest high correlation. However these correlations include spatial different intensity profiles. In next section we show the results of peak analysis.

## 5.2 Analysis of XPS Spectra

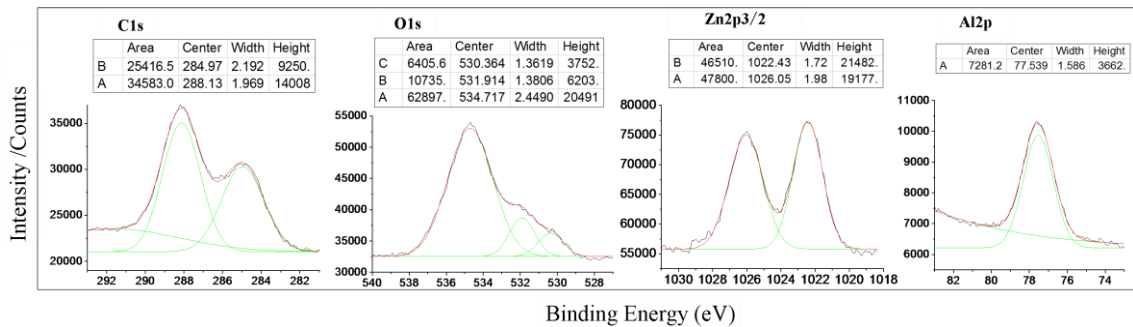


Fig.5. 3 XPS spectrum of C1s, O1s, Zn2p3/2 and Al2p at N5 were fitted out.

Elements of XPS spectrum from N1 to N9 were exhibited in fig.5.2, respectively. Silicon was scarcely, and Si hadn't been fitted. In fig.5.3, XPS spectra of C1s, O1s, Zn2p3/2 and Al2p at N5 were fitted out, and Si 2p peak is weak to ignore. The splitting peaks and characteristic factors were indicated out:

- 1) C1s was splitted to two (A and B) peaks: Binding energy of peak center of B was 285.0eV, what showed as the factor of "Center" in table of fig.5.3-C1s. The standard point of these data is C1s (285.0eV). The width at half maximum height of peak B was 2.2eV, what exhibited as factor of "Width". The integral value of intensity of peak B was 25416, what exhibited as factor, "Area". The intensity of peak center of B was 9250, what exhibited as factor, "Height". The factors of fitted peak A also showed in the table at fig.5.3-C1s.
- 2) O1s was a boarding peak. At high binding energy side, there was a strong satellite marked to A. From 530eV to 534eV, there should be two different combinative states oxygen, at least. The factors of fitted peaks of oxygen were exhibited in the table of fig.5.3-O1s.
- 3) Spectrum of Zn2p3/2 was fitted to two peaks, clearly. The factors of fitted peaks of zinc were exhibited in the table of fig.5.3-Zn2p3/2.
- 4) Spectrum of Al2p was single. The factors of fitted peaks of alumina

were exhibited in the table of fig.5.3-Al2p.

The fitting results of binding energy of peaks from N1 to N9 were showed in fig.5.4; and the fitting results of intensity of fitting out peaks from N1 to N9 were showed in fig.5.5

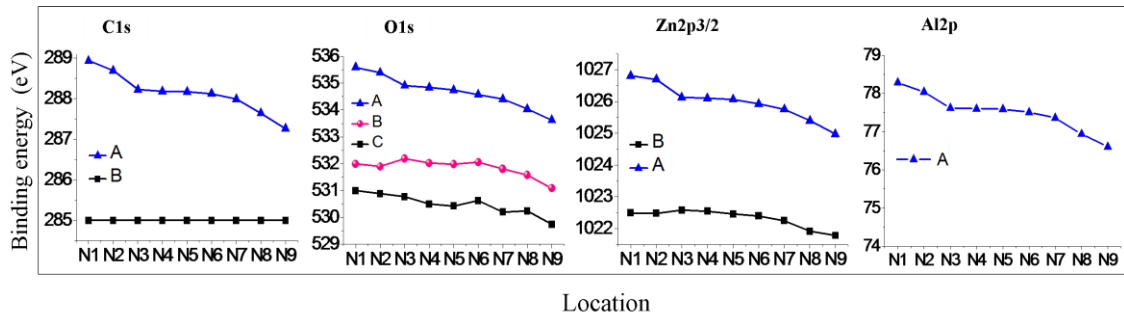


**Fig.5.4 Spatial changes of the binding energy of C1s, O1s, Zn2p3/2 and Al2p.**

Fig.5.4 showed the spatial change of the binding energy of C1s, O1s, Zn2p3/2 and Al2p from N1 to N9. The peaks at 285.0eV of C1s are due to adsorbed carbon oxide, which was fixed as the standard of the spectra. C1s at 288eV region showed stepwise structure. The stepwise structures were observed in all spectra with higher binding energies. The other peaks with lower energies of O1s and Zn2p3/2 showed monotonous decrease as changing the position from N1 to N9.

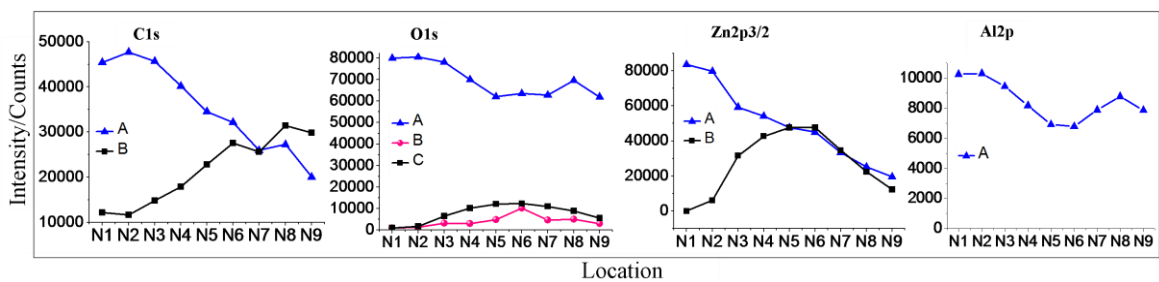


**Fig.5.5 The spatial symmetry of XPS spectrum intensity of C1s, O1s, Zn2p3/2 and Al2p**

Fig.5.5 showed the spatial profiles of integrated peak intensities of analyzed peaks. Intensity profiles of two peaks at A and B of C1s showed complemented structures with odd symmetry. The summation of these peaks was almost constant. Intensity profiles of O1s include two groups. The symmetry of these profiles is all even symmetry. However, the profiles with lower energy, peak-B and Peak-C of O1s, showed even symmetrical, on the other hand, the profiles with higher energy, peak-A of O1s, showed the sum of

even symmetrical and odd symmetrical. Intensity profiles of Zn2p<sub>3/2</sub> include even symmetry of the profile with lower energy, peak-B of Zn2p<sub>3/2</sub>, and odd symmetry of that with higher energy, peak-A of Zn2p<sub>3/2</sub>. The summation of these is not constant. The intensity in the half from N6 to N9 decreased linearly. The intensity profile of Al2p showed the sum of even symmetrical and odd symmetry at high energy side of normal Al<sub>2</sub>O<sub>3</sub> (74.4eV).

## 5.3 Discussion

We discussed the states of special excited zinc film and the spatial symmetry of zinc, and we calculated the important independence parameters, Q, T, and  $\Delta$  of charge transfer mechanism.

### 5.3.1 The states of zinc

From fig.5.6b, the XPS spectrum of surface slightly oxidized mental zinc (Zn, ZnO) and N5 in fig.5.2 was showed. There were two satellites at the high binding energy side of Zn2p at N5. To elucidated the states of zinc in our special film. Here we consider the 2p XPS of transition mental compounds, firstly. Experimental data observed by Rosencwaig et al. [37]. There is no satellite peak in the Zn2p of ZnF<sub>2</sub> where the 3d shell is filled. However, the satellite of 2p XPS from CuF<sub>2</sub> to MnF<sub>2</sub> occurs on the higher binding energy side of the main peak. It is now well established that it originates from the charge transfer between the ligand 2p and metal 3d orbital. From other researches, the properties of strong correlation and high temperature superconductivity directly related to half filled 3d orbital of the transition metals. However, how can distinguish the 3d full filled states and 3d half filled state? Fig.5.6a showed X-ray photo spectroscopy of Cu2p and O1s in Cu, Cu<sub>2</sub>O and CuO [38][39]. Metal Cu and Cu<sub>2</sub>O with 3d<sup>10</sup> showed almost the same spectrum of Cu2p, but CuO with 3d<sup>9</sup>(orbital of 3d is not full filled.) showed different spectrum of Cu2p to Cu and Cu<sub>2</sub>O. The peak at high binding energy side was identified as the peak, what due to 2p<sup>5</sup>3d<sup>9</sup> final state that the movement of the holes did not occur. The peak of low binding energy side could be fitted to two peaks. The fitting peak at high binding energy side is final state of 2p<sup>5</sup>3d<sup>10</sup>L, what the movement of hole was occur from Cu3d to O2p with the photoelectron emission. Components what form the sharp rise at the low binding energy side, is 2p<sup>5</sup>3d<sup>10</sup> final state, that is derived from a hole in the valence band is moved to O2p band of adjacent site.

However, 3d orbit of ZnO and Zn is full filled; and new peak at high energy side isn't exhibited. The electron transition from O2p to Zn3d couldn't happen, and there is no satellite peaks to identify the 3d<sup>10</sup>L state of high binding energy side in the X-ray photoelectron spectroscopy. If 3d is half filled, new peaks at the high binding energy side could be exhibited, what is caused by electron transition between ligand to transition metal. From this we can infer

that, in the figures, the new peaks at the high binding energy side of  $Zn^*$  could be exhibited, what caused by half filled of  $Zn^* 3d^n$  ( $n < 10$ ) orbits. We considered the peak A of  $Zn2p_{3/2}$  at high energy side was originated to final state of  $Zn2p^53d^9$ , and the peak B of  $Zn2p_{3/2}$  must originated to the final states of  $Zn2p^53d^{10}$  or  $Zn2p^53d^{10}\underline{L}$ . In other experiments, the relative intensity of peak A and peak B was changed by irradiation of strong X-ray, and it was reported between  $3d^9$  and  $3d^{10}\underline{L}$ .

We considered peak A of  $Zn2p_{3/2}$  originated by final state of  $Zn2p^53d^9$ , peak B of  $Zn2p_{3/2}$  originated by the final state of  $Zn2p^53d^{10}\underline{L}$ .

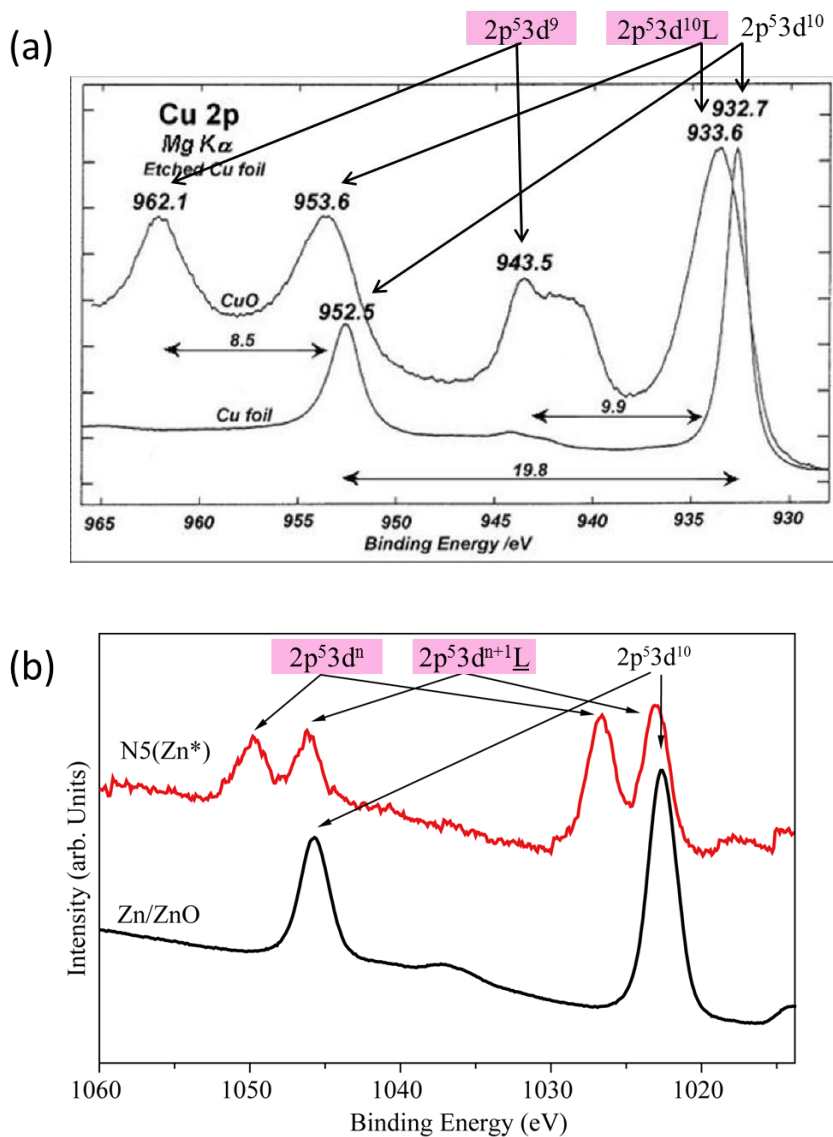


Fig.5.6a 2p XPS spectrum of Cu foil and CuO [40]; Fig.5.6b 2p XPS spectrum of Zn/ZnO and N5( $Zn^*$ ), N5 in Figure 1 at center of the sample ( $Zn^*$ : Excited state of zinc).

### 5.3. 2 Theoretical calculation of CT

The correspondence between initial state, final state and XPS spectrum of charge transfer process was showed in fig.5.6. Factors of charge transfer energy ( $\Delta$ ), mixing energy (T) and coulomb interaction energy between 3d and inner-holes (Q) are the most important factors in charge transfer process. In figure 6, we show an ionic state energy diagram of XPS. From charge transfer theory by A. Kotani and K. Okada [41], T,  $\Delta$ , and Q following series of equations, that is established in section 4.6.

The peak interval,  $\delta E_B$  of final state of  $f_1$  and  $f_2$  and intensity ratio,  $R = \frac{I_{f2}}{I_{f1}}$  can be written in equivalence equation (a) and (b) as following:

$$\delta E_B \equiv E_{f2} - E_{f1} = \sqrt{\Delta_f^2 + 4T^2} = \sqrt{(\Delta - Q)^2 + 4T^2} \quad (a)$$

$$R = \frac{I_{f2}}{I_{f1}} = \tan^2(\theta_f - \theta_g) \quad (b)$$

$$= \tan^2\left(\arccos \frac{\sqrt{\Delta_f^2 + 4T^2} - \Delta_f}{2T} - \arccos \frac{\sqrt{\Delta^2 + 4T^2} - \Delta}{2T}\right)$$

$$= \tan^2\left(\arccos \frac{\delta E_B - (\Delta - Q)}{2T} - \arccos \frac{\sqrt{\Delta^2 + 4T^2} - \Delta}{2T}\right)$$

**Table 5.1** The independent parameter of  $\Delta$  and T were calculated out from N1 to N9

|    | The charge transfer parameters ( $\Delta$ , T, Udc) |       |     |          |            |                |                |      | Ground state |       | Final state            |           |                            |                                  |
|----|---|-------|-----|----------|------------|----------------|----------------|------|--------------|-------|------------------------|-----------|----------------------------|----------------------------------|
|    | $\delta E_B$  | I+/I. | Q   | $\Delta$ | $\Delta f$ | ( $\theta_f$ ) | ( $\theta_g$ ) | T    | Eg           | $d^n$ | $d^{n+1}\underline{L}$ | $2p^5d^n$ | $2p^5d^{n+1}\underline{L}$ | $2p^5d^{n+1}\underline{L} + E_g$ |
| N1 | 4.31  | 60    | 5.5 | 1.20     | -4.30      | 87.35          | 4.72           | 0.10 | -0.01        | 0.00  | 1.20                   | 0.00      | -4.30                      | -4.31                            |
| N2 | 4.20  | 7.31  | 5.5 | 1.34     | -4.16      | 81.72          | 12.28          | 0.31 | -0.07        | 0.00  | 1.34                   | 0.00      | -4.16                      | -4.23                            |
| N3 | 3.55  | 1.78  | 5.5 | 2.23     | -3.27      | 68.82          | 15.82          | 0.69 | -0.19        | 0.00  | 2.23                   | 0.00      | -3.27                      | -3.46                            |
| N4 | 3.55  | 1.19  | 5.5 | 2.36     | -3.14      | 64.98          | 17.54          | 0.83 | -0.26        | 0.00  | 2.36                   | 0.00      | -3.14                      | -3.40                            |
| N5 | 3.60  | 0.91  | 5.5 | 2.43     | -3.08      | 62.48          | 18.87          | 0.94 | -0.32        | 0.00  | 2.43                   | 0.00      | -3.08                      | -3.40                            |
| N6 | 3.52  | 0.92  | 5.5 | 2.50     | -3.00      | 62.39          | 18.18          | 0.92 | -0.30        | 0.00  | 2.50                   | 0.00      | -3.00                      | -3.30                            |
| N7 | 3.50  | 0.91  | 5.5 | 2.54     | -2.96      | 61.85          | 18.22          | 0.94 | -0.31        | 0.00  | 2.54                   | 0.00      | -2.96                      | -3.27                            |
| N8 | 3.47  | 1.05  | 5.5 | 2.50     | -3.00      | 63.22          | 17.52          | 0.88 | -0.28        | 0.00  | 2.50                   | 0.00      | -3.00                      | -3.28                            |
| N9 | 3.19  | 1.55  | 5.5 | 2.67     | -2.83      | 65.28          | 14.40          | 0.73 | -0.19        | 0.00  | 2.67                   | 0.00      | -2.83                      | -3.02                            |

The peak intervals  $\delta E_B$  and intensity ratio  $R = \frac{I_{f2}}{I_{f1}}$  is known from source data of XPS in fig.5.4, fig.5.5 and fig5.6b. From equation (a) and (b), unknown numbers of  $\Delta_f$ , T,  $\theta_f$  and  $\theta_g$  can be rewrite to T,  $\Delta$ , Q. In the zinc excited film, the ligand should be carbon. The value of Q is not dependent on the metal ions, and Q is reduced with electrical negative degrees of ligand to transition metal compound [42]. In this calculation, we supposed Q=5.5eV, T and  $\Delta$  can be calculated out.

From the energy difference,  $\delta E_B$ , and peak intensity ratio,  $I_+/I_-$ , between  $2p^53d^9$  and  $2p^53d^{10}\underline{L}$ , the  $\Delta$  and T were estimated. The results were exhibited in table 5.1. In the region where the intensity of  $2p^53d^{10}\underline{L}$  becomes large,  $\Delta$  becomes small,  $1.2\text{eV} < \Delta < 2.7\text{eV}$ , and T becomes small, too,  $0.1\text{eV} < T < 0.9\text{eV}$ , respectively.

### 5.3.3 The spatial symmetry of excited zinc film

The correlation between analyzed profiles is useful to decide the interaction between each element. From fig.5.4 and fig.5.5, the electron state of peak-A in C1s correlates with the electron state of peak-A in  $\text{Zn}2p_{3/2}$ . The electron state of Al2p correlates with the electron state of peak-A of O1s. The state of peak-C in O1s correlates with peak-B of  $\text{Zn}2p_{3/2}$ . These correlations suggest the combination of the origins of these states. The satellites at high binding energy side of zinc were odd symmetry, and the peaks at low binding energy side of zinc were even symmetry. We can realize that the initial state of  $\text{Zn}3d^9$  is odd symmetry, but the initial state of  $\text{Zn}3d^{10}\underline{L}$  shows even symmetry. The different spatial symmetry of  $\text{Zn}3d^9$  and  $\text{Zn}3d^{10}\underline{L}$  originated from different force [43].

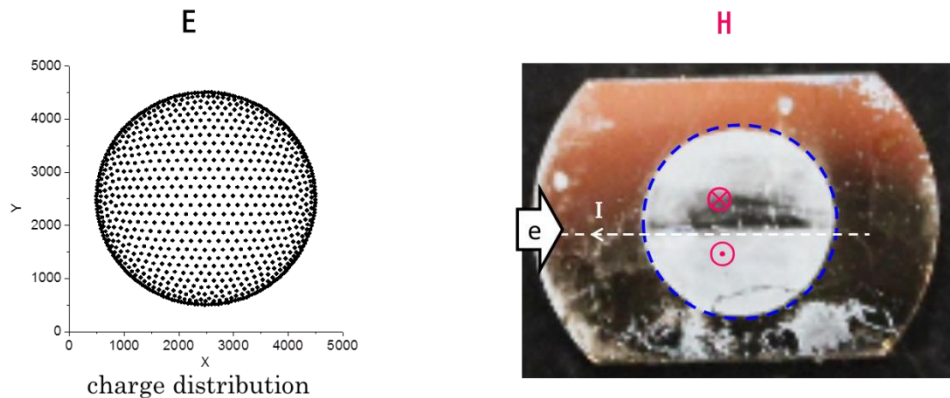


Fig.5.7 The distribution of electric field and magnetic field.

The external fields on earth just gravitational field, magnetic field and electric field can be considered. Fig.5.7 showed the distribution of electric field and magnetic field. From sample preparation, there is an even symmetry electric field be made out by electron incident. The even symmetry of  $Zn3d^{10}\underline{L}$  correlated to electric field. There was micro electric current occurred on the sapphire substrate, because of electron incident, and the direction of the micro electric currents were same. The same direction micro electric current made the same direction of magnetic field. So, the odd symmetry of  $Zn3d^9$  could correlate to magnetic field.

#### ***5.3.4. The structural instability of excited Zn film***

Charge conservation in excited zinc atom suggests combination between two  $Zn3d^9$  and  $C^{2-}$  ions. The size of  $C^{2-}$  is almost comparable to that of oxygen atom. If the electrons transfer from  $C^{2-}$  to  $3d^9$ , the size of the carbon shrinks to 0.154 nm from 0.25 nm. Therefore the charge transfer induces a vacancy due to the rapid diffusion of carbon. In our experiment, the sample showed high mobility of the constituting elements.

# *Chapter 6 THE CORRELATION BETWEEN ELEMENTS*

## *6.1 The Results of 192 Points by XPS*

From fig.6.1, center of the sample is thin than other area. And upper side is thin than bottom. In fig.6.2, the XPS spectra around h1 are different to other measuring area. The XPS spectra of Zn3d are more different than other spectra of elements, and C1s is similar to Zn3d, next is O1s. The sample was measured after 50 days, which was measured again in 192 points by XPS. And the results of h1~h16 were shown in fig.6.2. h1, h2, and h3 is very different between others. And the electronic incident from left edge in fig.6.1. The features were described below.

- 1) The satellite of zinc was present just at the outer peripheral portion.
- 2) The satellite is not uniformly distributed, and there was a strong correlation with the incident electron direction.
- 3) The XPS data of zinc, carbon, oxygen, aluminum and silicon showed strong correlation.

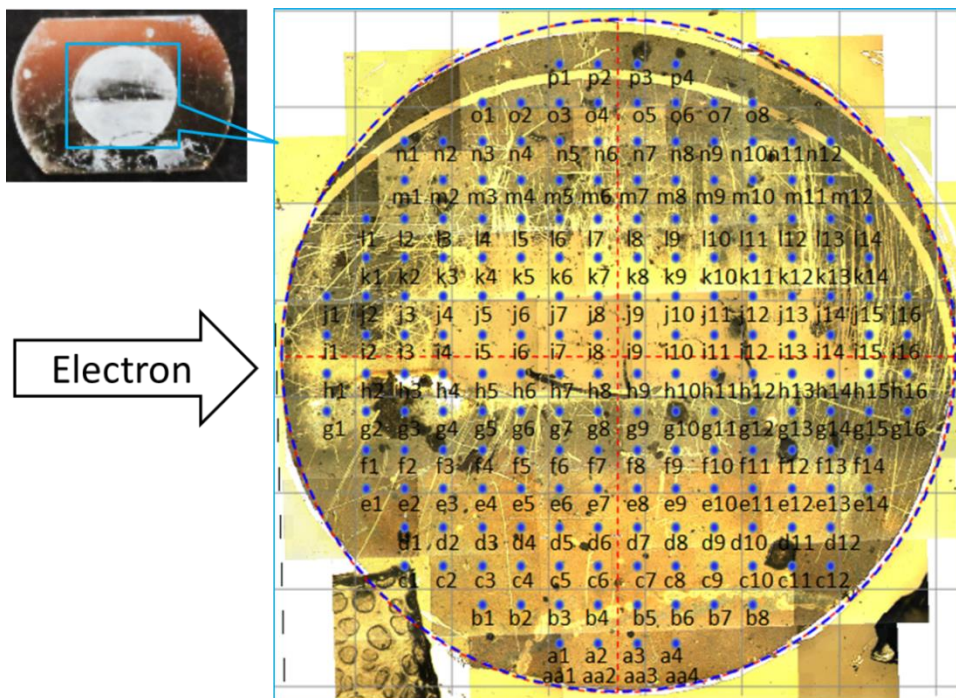


Fig.6.1 192 measuring points average distribute on “Sample 100”.

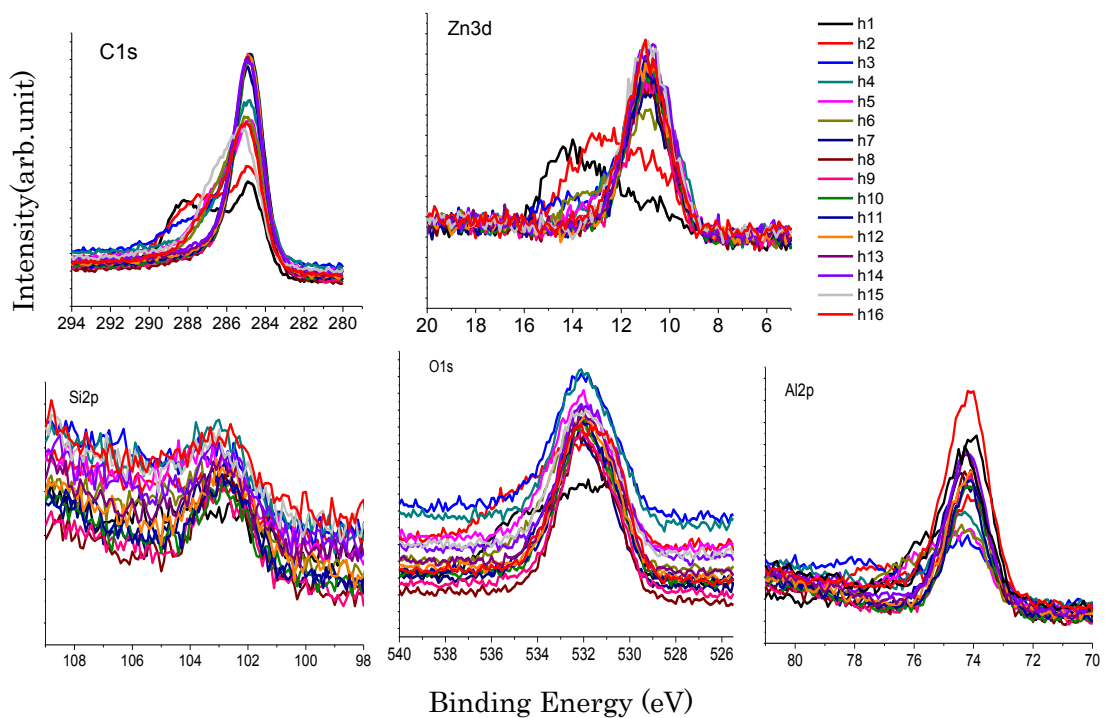
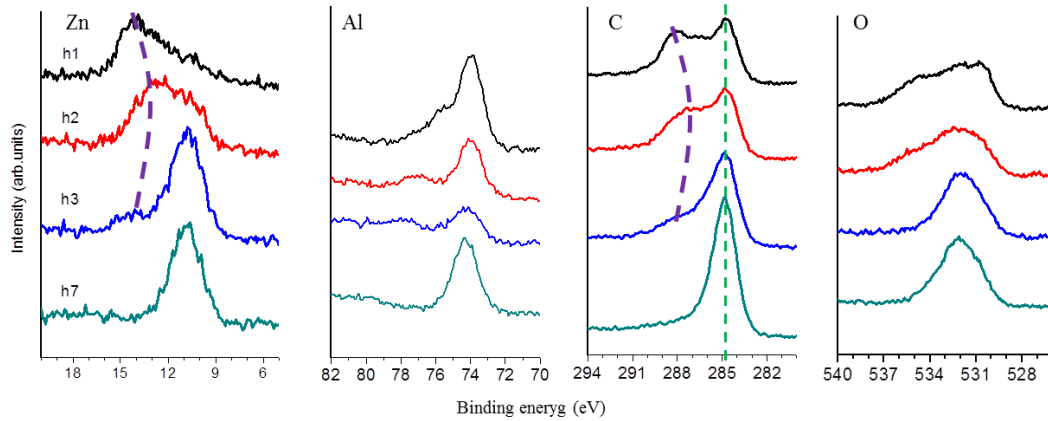


Fig.6.2 192 points that average distribution on “Sample 100”. Measuring point h1~h16 is lateral average distribution at the center of “sample 100”. XPS spectrum of C1s, O1s, Zn3d, Al2p and Si2p were display.

## 6.2 The Correlation between Constituent Elements



**Fig.6.3** XPS spectra of h1, h2, h3, and h7 of Zn3d, Al2p, C1s, and O1s were shown.

In fig.6.3, the XPS spectra of h1, h2, h3 and h7 of Zn3d, Al2p, C1s, and O1s were shown. Satellite peak of Zn and C at the high binding energy side is in similar variation. The spatial distribution of bound states of 192 points was shown in fig.6.4. The satellite peak concentrated on the left edge of the sample, and all of the elements unevenly distributed. The elements distribution of integrating sample surface was shown in fig.6.5. Fig.6.5 corresponds an elements contend distribution map.

The thin film is thin at the substrate center, but it is thick at upper and down of the thin film. Zinc with satellite state was present only in the electron incidence side of the sample. Distribution of all the zinc atoms that contain main peak and satellite of zinc, top and bottom of the perpendicular to the incident electron direction were more than in the center. The quantity of Al and Si decreased from center to top and bottom of the perpendicular to the incident electron direction. Oxygen distributes almost uniform in the sample surface.

From chapter 5, the satellite peak at the high binding energy side corresponds to ground state of Zn3d<sup>9</sup>. The spatial density distribution of binding carbon and Zn\* showed a positive correlation. It is proved that, the ligand of zinc excited state is carbon. The spatial density distribution of aluminum and Zn\* showed an inverse correlation, there was a displacement reaction between excited state zinc atoms to aluminum atoms. The excited state of zinc atoms was discovered after the film was generated 357 days ago.

Compare to chapter 5, the satellites of zinc at the high binding energy side existed. The zinc excited state with a permanent long lifetime. Though, the excited states on the film surface are unstable.

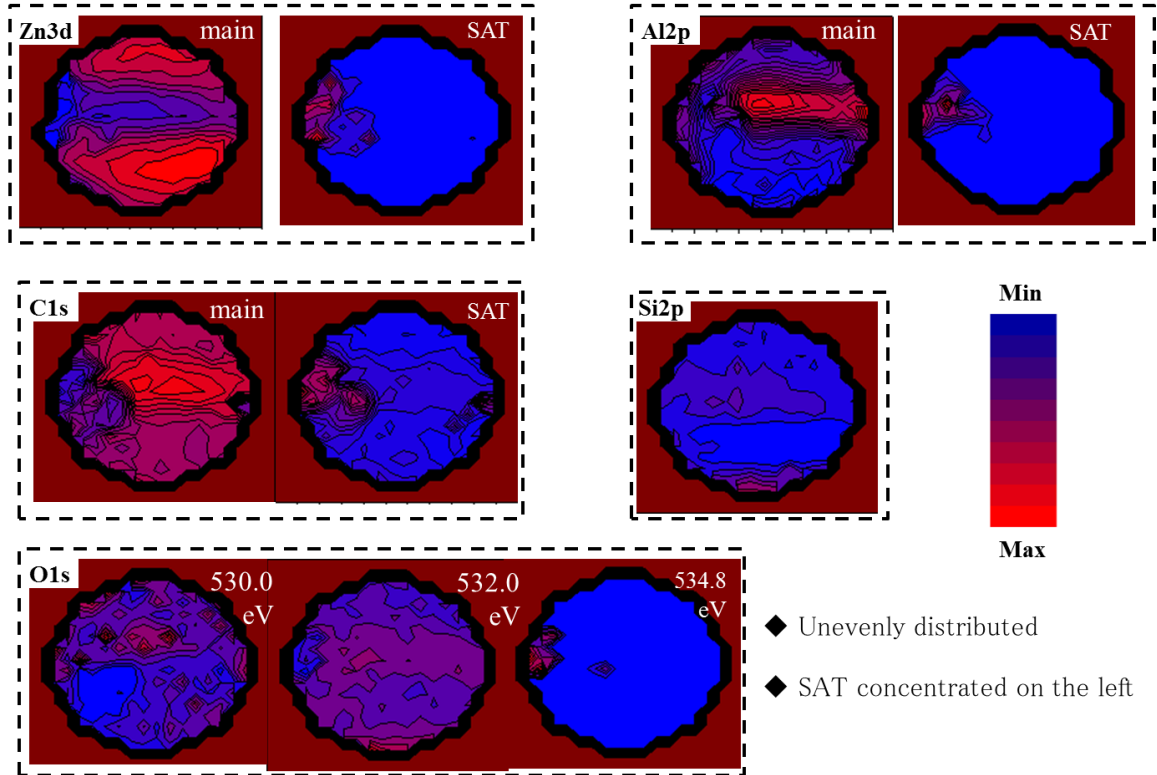


Fig.6.4 Distribution of the different states of elements on “sample 100”, after it is created 357days ago.

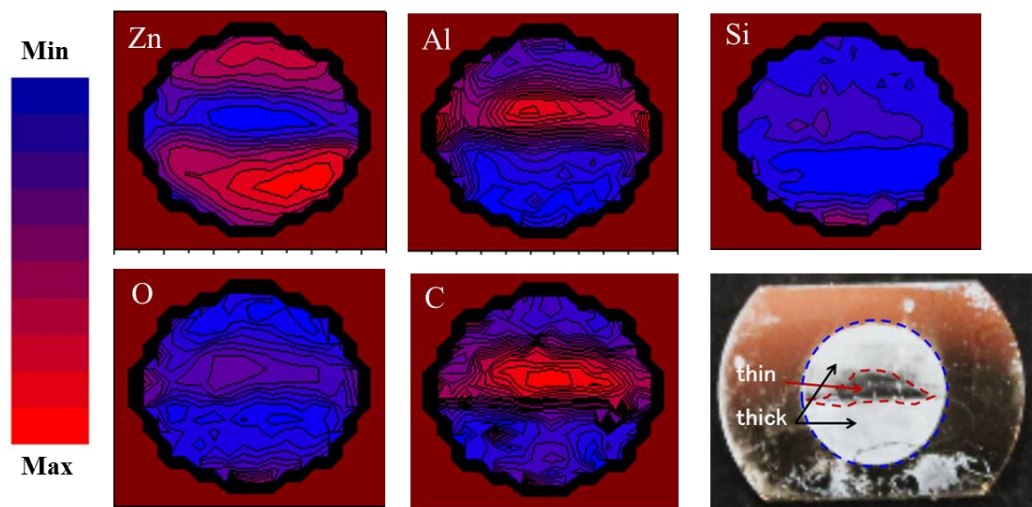


Fig.6.5 Elements distribution of “sample 100” after it is created out 357days ago.

### 6.3 The Time and Spatial Distribution of Films

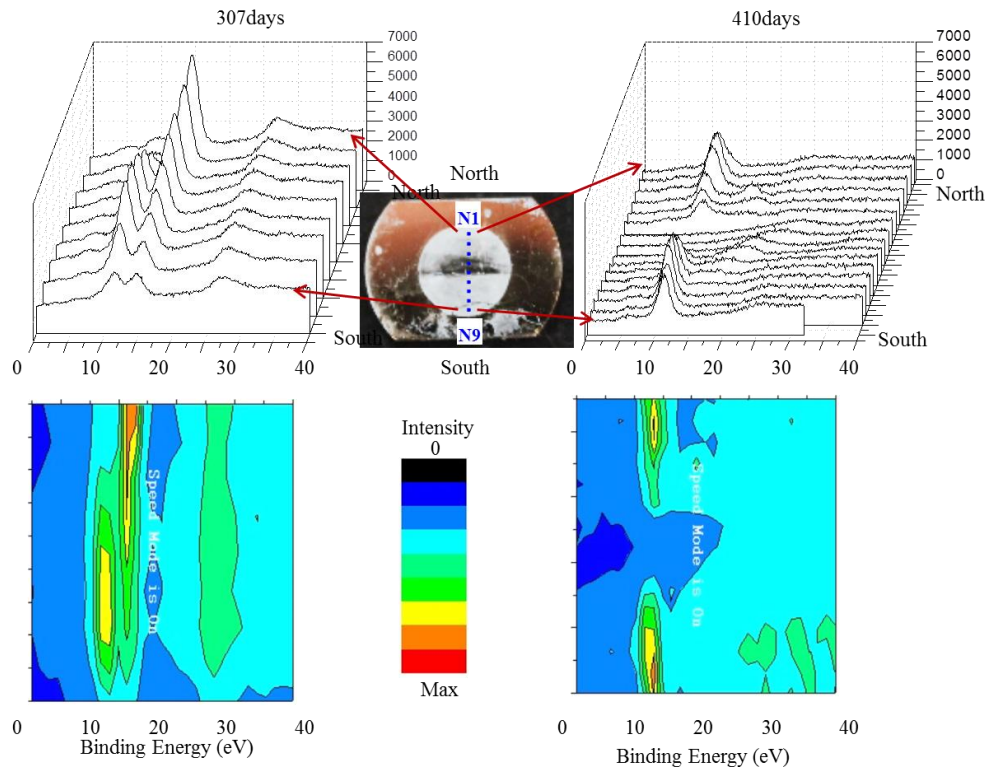


Fig.6.6 The time dependences of XPS spectra distribution at vertical direction through center of the sample.

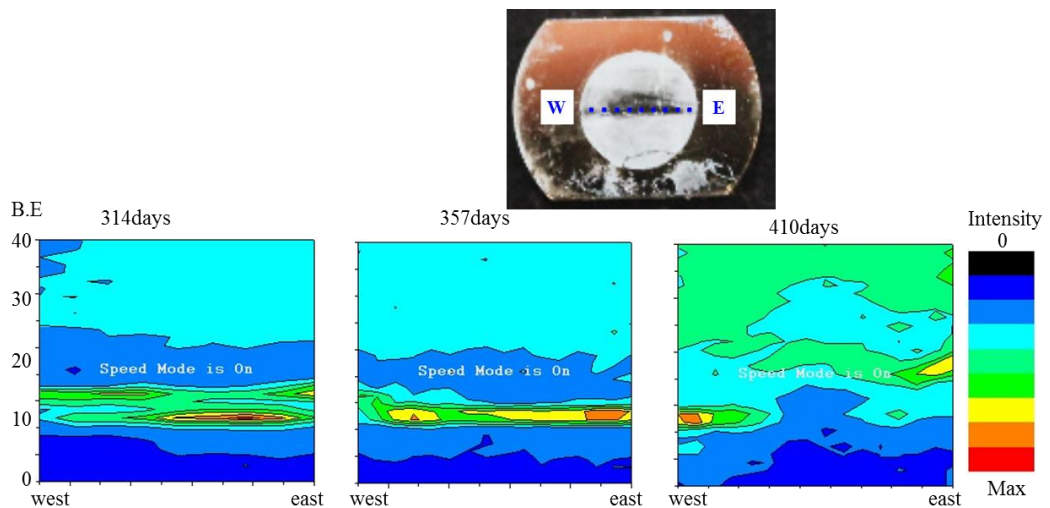


Fig.6.7 The time dependences of XPS spectra distribution on lateral direction through center of the sample.

The time dependences of XPS spectra distribution at vertical direction through center of the sample was shown in fig.6.6. The time dependences of XPS spectra distribution on lateral direction through center of the sample was shown in fig.6.7. From fig.6.6 and 6.7 we can conclude out these conclusions:

1. Excited states change by the time variation.
2. Excited states change by the spatial variation.
3. The peak intensity decreased, while the peak shifted to high binding energy side.
4. Excited state is non-rotationally symmetric distribution.
5. The excited state is quasi-stable state.

## *Chapter 7 CONCLUSIONS*

This paper presents a result of the challenge of the excitation of inner-core electron system with long lifetime of excited zinc films. The advanced zinc films with excited inner-core electron,  $3d^9$ , were formed by surface ion-recombination process controlled by the collision energy.

We report experimental results of XPS measurements of 9 points along vertical direction from N1 to N9. The most pronounced features are existence of the satellites, which are about 4eV higher than the main lines. This is the proof of the existence of 3d-hole ground state,  $Zn3d^9$ , which is the same mechanism of CuO. The measured XPS spectra apparently depend on the location in the sample. These satellites are due to the charge transfer mechanism of electron from the ligand to  $3d^9$ . According to the charge transfer mechanism proposed by A. Kotani and K. Okada, it was clarified that the origins of these peaks are  $3d^{10}\underline{L}$  for the main peak and  $3d^9$  for the satellite, respectively. The samples contain Zn, Al, O, C and Si. The surface densities of these elements depend on the location of the sample. In the analysis along the vertical direction, intensity profile of  $Zn3d^9$  showed odd functional symmetry and that of  $Zn3d^{10}\underline{L}$  showed even functional symmetry. Only the intensity profile of C1s (288eV) showed the same spatial correlation with  $Zn3d^9$ . This is the reason that the ligand for  $Zn3d^9$  is Carbon, not Oxygen. The other elements roughly show the even functional symmetry.

We analyzed experimental data by using Kotani and Okada's theoretical model. From the energy difference,  $\delta E_B$ , and peak intensity ratio,  $I^+/I^-$ , between  $2p^53d^9$  and  $2p^53d^{10}\underline{L}$ , the energy for charge transfer,  $\Delta$ , and mixing energy,  $T$ , were estimated. In the region where the intensity of  $2p^53d^{10}\underline{L}$  becomes large,  $\Delta$  becomes small,  $1.2 < \Delta < 2.7$ , and  $T$  becomes small, too,  $0.1 < T < 0.9$ , respectively. In this calculation, we supposed  $U_{dc} = 5.5$  eV. The excited zinc films also showed high mobility of the constituting elements which correlated to  $C^{2-}$ . We conclude that the excited zinc films have 3d-hole,  $3d^9$ , with almost permanent lifetime and  $3d^9$  combine with carbon. Although the detailed mechanism of the long lifetime of the inner-core excited zinc atoms is not clear at the present time, this material suggests the high potential for the advanced application in wide area.

## *Reference*

- [1] Atkinson, G., S. Dietz, and E. Neumayer (2009). Handbook of Sustainable Development. Edward Elgar Publishing, ISBN 1848444729.
- [2] Hasna, A. M. (2007). "Dimensions of sustainability". Journal of Engineering for Sustainable Development: Energy, Environment, and Health 2 (1): 47–57. doi:10.3992/2166-2517-1.2.47.
- [3] Callister, Jr., Rethwisch. "Materials Science and Engineering-An Introduction" (8th ed.). John Wiley and Sons, 2009 P5-6.
- [4] Hübler, Arved; et al. (2011). "Printed Paper Photovoltaic Cells". Advanced Energy Materials 1 (6): 1018–1022. doi:10.1002/aenm.201100394.
- [5][http://www.ml.seikei.ac.jp/tsubomura/education/muki2/muki2\\_4.pdf#search='%E9%81%B7%E7%A7%BB%E9%87%91%E5%B1%9E+%E5%85%83%E7%B4%A0+%E6%80%A7%E8%B3%AA+%E8%B3%87%E6%BA%90'](http://www.ml.seikei.ac.jp/tsubomura/education/muki2/muki2_4.pdf#search='%E9%81%B7%E7%A7%BB%E9%87%91%E5%B1%9E+%E5%85%83%E7%B4%A0+%E6%80%A7%E8%B3%AA+%E8%B3%87%E6%BA%90')
- [6] Cotton, F. Albert; Wilkinson, G.; Murillo, C. A. (1999). Advanced Inorganic Chemistry (6th ed.). New York: Wiley, ISBN 0471199575.
- [7] [http://en.wikipedia.org/wiki/Transition\\_metal](http://en.wikipedia.org/wiki/Transition_metal)
- [8] P. Jeffrey Hay and Thom H. Dunning, Jr. Richard C. Raffennetti, Electronic states of Zn<sub>2</sub>. Ab initio calculations of a prototype for Hg<sub>2</sub>, The Journal of Chemical Physics, Vol. 65, No.7, October 1976.
- [9] Hamasaki, M., Yamaguchi, M., Kuwayama, M. and Obara, K. (2011) A New Approach for Sustainable Energy Systems Due to the Excitation of Inner-Core Electrons on Zinc Atoms Induced by Surface-Ion-Recombination. AIP Conference Proceeding, 1415, 43-50. <http://dx.doi.org/10.1063/1.3667216>
- [10] Obara, M., Hamasaki, M., Manaka, H. and Obara, K. (2011) Slowly Relaxing Structural Defects of Zinc Films with Excited States Induced by Ion Recombination Processes. Advanced Materials Research, 277, 11-20. <http://dx.doi.org/10.4028/www.scientific.net/AMR.277.11>
- [11] Hay, P.J., Dunning Jr., T.H. and Raffennetti, R.C. (1976) Journal of Chemical Physics, 65, 2679.
- [12] Siegbahn, K., Nordling, C., Fahlman, A., Nordberg, R., Hamrin, K., Hedman, J., Johansson, G., Bergmark, T., Karlsson, S., Lindgren, I., and Lindberg, B. (1967) ESCA-Atomic, Molecular and Solid State Structure Studied by Means of Electron Spectroscopy, Nova Acta Regiae Soc. Sci. Ups., Ser IV, 20.
- [13] [http://en.wikipedia.org/wiki/Excited\\_state](http://en.wikipedia.org/wiki/Excited_state)
- [14] van Setten, Uijttewaal, de Wijs and de Groot (2007). JACS 129: 2458–2465.

- [15] P. Jeffrey Hay and Thom H. Dunning, Jr. Richard C. Raffanetti, Electronic states of Zn<sup>2+</sup>. Ab initio calculations of a prototype for Hg<sup>2+</sup>, *The Journal of Chemical Physics*, Vol. 65, No.7, October 1976.
- [16] K. Okada, A. Kotani, Charge transfer satellites and multiplet splitting in X-ray photoemission spectra of late transition metal halides, *Journal of Electron Spectroscopy and Related Phenomena*, 1992.6.
- [17] Susumu Asada, Satoru Sugano, Satellites in X-ray photoelectron spectra of transition-metal compounds, *Journal of the Physical Society of Japan*, 41(4), 1976.10.
- [18] Ehrlich, G. and Hudda, G. (1966) Atomic View of Surface Self-Diffusion: Tungsten on Tungsten. *The Journal of Chemical Physics*, 44, 1039-1049.  
<http://dx.doi.org/10.1063/1.1726787>
- [19] Mitsugi Hamasaki, Masumi Obara, Kozo Obara, Hirotaka Manaka, A quantum dynamic approach to the condensation processes of zinc atoms by the inner-core excitation due to ion-recombination, *International Journal of Technology*, Vol. 2, Issue 2, July 2011, PP.130-138.
- [20] P.S. Bagus, A. J. Freeman, F. Sasaki, Prediction of new multiplet structure in photoemission experiments, *Physical Review Letters*, 1973.4, P850-853.
- [21] Harris, D.C.; Bertolucci, M.D. (1978). *Symmetry and Spectroscopy*. Oxford University Press. ISBN 0-19-855152-5.
- [22] Cotton, F.A. (1990). *Chemical Applications of Group Theory* (3rd ed.). Wiley. ISBN 978-0-471-51094-9.
- [23] Qiongqiong Hou, Fanjie Meng and Jiaming Sun, Electrical and optical properties of Al-doped ZnO and ZnAl<sub>2</sub>O<sub>4</sub> films prepared by atomic layer deposition, Hou et al. *Nanoscale Research Letters* 2013, 8:144
- [24] Shicheng Yan, He Yu, Nanyan Wang, Zhaosheng Li and Zhigang Zou, Efficient conversion of CO<sub>2</sub> and H<sub>2</sub>O into hydrocarbon fuel over ZnAl<sub>2</sub>O<sub>4</sub>-modified mesoporous ZnGaNO under visible light irradiation, *Chem. Commun.*, 2012,48, 1048-1050
- [25] Koopmans, T. *Physica* 1933, 1, 104-113.
- [26] Froese Fischer, Charlotte (1987). "General Hartree-Fock program". *Computer Physics Communication* 43 (3): 355-365.  
[http://en.wikipedia.org/wiki/Hartree%E2%80%93Fock\\_method](http://en.wikipedia.org/wiki/Hartree%E2%80%93Fock_method)
- [27] D. A. Shirley, *Electron Spectroscopy: Theory, Techniques and Applications*, Vol. 1, Academic Press (1978).
- [28] G.L. Miessler and D.A. Tarr, *Inorganic Chemistry* (Prentice-Hall, 2nd edn 1999) [ISBN 0138418918], pp. 358-360
- [29] T. Engel and P. Reid, *Physical Chemistry* (Pearson Benjamin-Cummings, 2006) [ISBN 080533842X], pp. 477-479

- [30] Charles S. Fadley, Atomic-Level Characterization of Materials with Core- and Valence-Level Photoemission: Basic Phenomena and Future Directions  
<http://www.physics.ucdavis.edu/fadleygroup/ALC07.Fadley.final.preprint.withfigs.pdf>
- [31] Veal & Paulikas: Phys. Rev. B 31 (1985) 5399.
- [32] Radiative Corrections, Peter Schnatz. Accessed 08 March 2013.
- [33] Fuggle, J.C., Hillebrecht, F.U., Zolnierik, Z., Lasser, R., Freiburg, C., Gunnarsson, O., and Schonhammer, K. (1983) Phys. Rev. B, 27,7330.
- [34] Dahlang Tahir and Sven Tougaard, Electronic and optical properties of Cu, CuO and Cu<sub>2</sub>O studied by electron spectroscopy, 2012 J. Phys.: Condens. Matter 24 175002. doi:10.1088/0953-8984/24/17/175002
- [35] Frank de Groot, Akio Kotani, Core Level Spectroscopy of Solids, CRC Press, Taylor & Francis Group, 2008.
- [36] Veal and Paulikas (1985) Final-State Screening and Chemical Shifts in Photoelectron Spectroscopy. Physical Review B,31, 5399.
- [37] Rosencwaig, A., Wertheim, G.K. and Guggenheim, H.J. (1971) Origins of Satellites on Inner-Shell Photoelectron Spectra. Physical Review Letters, 27, 479.  
<http://dx.doi.org/10.1103/PhysRevLett.27.479>
- [38] Rosencwaig, A. and Wertheim, G.K. (1971) Origins of Satellites on Inner-Shell Photoelectron Spectra. Physical Review Letters, 27, 479-481.  
<http://dx.doi.org/10.1103/PhysRevLett.27.479>
- [39] Tanaka, K. (1998) X-Ray Photoelectron Spectroscopy.
- [40] Tahir, D. and Tougaard, S. (2012) Electronic and Optical Properties of Cu, CuO and Cu<sub>2</sub>O Studied by Electron Spectroscopy. Journal of Physics: Condensed Matter, 24, 175002.  
<http://dx.doi.org/10.1088/0953-8984/24/17/175002>
- [41] Frank de Groot, Akio Kotani, Core Level Spectroscopy of Solids, CRC Press, Taylor & Francis Group, 2008.
- [42] Okada, K. (2004) Changes in the Electronic State of the Copper Oxide and Cu 2p XPS by Doping.
- [43] Fazelzadeh, S.A. and Ghavanloo, E. (2012) Nonlocal Anisotropic Elastic Shell Model for Vibrations of Single-Walled Carbon Nanotubes with Arbitrary Chirality. Composite Structures, 94, 1016-1022.  
<http://dx.doi.org/10.1016/j.compstruct.2011.10.014>
- [44] Kaupp M.; Dolg M.; Stoll H.; Von Schnering H. G. (1994), Oxidation state +IV in group 12 chemistry Ab initio study of zinc(IV), cadmium(IV), and mercury (IV) fluorides, Inorganic Chemistry 33(10): 2122.

## *Main Thesis*

1. Li Chen, Mitsugi Hamasaki, Hirotaka Manaka and Kozo Obara  
“Charge Transfer Mechanism and Spatial Density Correlation of Electronic States of Excited Zinc (3d<sup>9</sup>) Films”  
2014.5, Open Journal of Physical Chemistry, Vol. 4 No. 2 pp.44–51  
(Chapter 4,5,6,7)
2. Li Chen, Shinichiro Yamashita, Mitsugi Hamasaki, Hirotaka Manaka and Kozo Obara  
“Formation Processes of Zinc Excimer Thin Films due to Ion-recombination Processes”  
2014.6, Journal of Applied Mathematics and Physics, Vol. 2 No. 7 pp.449–456  
(Chapter 1,2,3,4,5)
3. M. Hamasaki, S. Miyashita, M. Obara, M. Kuwayama, Li Chen, H. Manaka, and K Obara  
“How We Can Produce Sustainable Society from Nanoscience and Nanotechnology for Next Generation-Prospects of Excited Dimers with Long Lifetime”  
2011.9, The 4<sup>th</sup> Nanoscience and Nanotechnology Symposium (NNS2011)
4. Kozo Obara, Li Chen, Koji Ikeda, Mitsugi Hamasaki, Masahiro Kuwayama, and Hirotaka Manaka  
“Spontaneous Structures of Zn Excimer Condensates Induce by Ion-recombination Processes under weak Magnetic Field”  
2012.8, The 6<sup>th</sup> International Conference on Spontaneous Coherence in Excitonic Systems ICSC-6, 3 [Pos14]
5. Li Chen, Shinichiro Yamashita, Mitsugi Hamasaki, Hirotaka Manaka and Kozo Obara  
“Formation Processes of Zinc Excimer Thin Films due to Ion-Recombination Processes -Excited States of Inner-core Electron System with “Permanent Lifetime”  
2012.9, International Union of Materials Research Societies – International Conference on Electronic Materials (IUMRS-ICEM), D-9-P24-004, pp. 114

6. Kozo Obara, Chen Li, Mitsugi Hamasaki, Mitsuomi Yamaguchi, Masahiro Kuwayama, Hirotaka Manaka  
“Condensation Processes of Long Lifetime Zn Excimers produced by Ion-recombination Processes”  
2012.9, International union of materials research societies - International Conference on Electronic Materials 2012
7. Li Chen, Koji Ikeda, Mitsugi Hamasaki, Masahiro Kuwayama and Kozo Obara  
“Charge Transfer Mechanism and Spatial Symmetry of Excited  $3d^n$  ( $n=9, 8$ ) Zinc Films”  
2013.9, The 12<sup>th</sup> Asia Pacific Physics Conference APPC12, A4
8. Kozo Obara, Li Chen, Koji Ikeda, Mitsugi Hamasaki, Masahiro Kuwayama and Hirotaka Manaka  
“Spontaneous coherent ring-structures of excitons induced by electron irradiation on oxide films contained inner-core electron excited zinc atoms at room temperature”  
2014 .4, The 7<sup>th</sup> international conference on spontaneous coherence in excitonic systems (ICSCE-7), PS2-24

## *Acknowledgements*

Thanks for Professor Kozo Obara teaching me various knowledge on exciton, X-ray photoelectron emission, Charge Transfer theory and so on. And Professor Obara guiding thesis of my research, giving me a lot of good ideas in my studying and live, teaching me ways of learning and many life skills. In addition, thank you for Professor Obara Kozo taking me to attend the international conferences to present our research, and then giving me so many suggestions and advices.

Thanks for Professor Norio Terada, Yuji Horie and Hideyo Nimiya guiding my thesis, giving me a lot of advice and suggestion for my research, helping me to correct the thesis. Thank you very much. Also, thanks for Researcher Hirotaka Manaka to giving me many suggestion and advice on my study and live time at these years.

Thanks for Doctor Mitsugi Hamasaki, Masumi Obara, Masahiro Kuwayama and Mitsuomi Yamaguchi to give me a lot of advice and suggestion for my research, helping me to correct the thesis. In addition, thanks for Yoshinaga Kazumi taking me to join the Science Partnership Project (SPP) and assume teaching assistant and teacher duties. And they are not only giving me so many advices for my research and live, but also giving me a lot of spirit support, even in searching job.

Thank you for all the members of Obara Group to help my study, teach me the Japanese, discussion our research together and give me a lot of suggestion. Especially, I would like to thank you for Miyashita, Kawabata, Ikeda and so on. Thanks for Division of Instrumental Analysis Natural Science Center for Research and Education giving the advice to examination sample by XPS, EPMA, SEM, XRD and so on. Especially, I would like to thanks for Kubo and Okura give me so much help to examination sample by XPS and EPMA.

In addition, I want to thanks for Rotary Yoneyama Memorial Foundation giving me scholarship in 2012 and 2013. Also, thanks for Kagoshima University giving me fee remission at my doctor course. If there are not economic supports, it would be more difficult of my doctor course. Finally, I would like to thanks for my parents and husband. Thanks for your care of me at economic and spirit in my life.